THE ASTROPHYSICAL JOURNAL, 445:62–79, 1995 May 20

RADIO PROPERTIES OF OPTICALLY SELECTED QUASARS

ERIC J. HOOPER AND CHRIS D. IMPEY
Steward Observatory, University of Arizona, Tucson, AZ 85721; ehooper@as.arizona.edu, cimpey@as.arizona.edu
CRAIG B. FOLTZ
Multiple Mirror Telescope Observatory, University of Arizona, Tucson, AZ 85721; cfoltz@as.arizona.edu
AND
PAUL C. HEWETT
Institute of Astronomy, University of Cambridge, Madingley Road, Cambridge, CB3 0HA, UK; phewett@mail.ast.cam.ac.uk
Received 1994 August 23; accepted 1994 November 29

ABSTRACT

Approximately one-quarter (256 objects) of the Large Bright Quasar Survey (LBQS) has been observed with the VLA at 8.4 GHz, resulting in 44 detections (17%) with a median 3 σ noise limit of 0.29 mJy. Quasars with radio luminosity detectable at this limit are underrepresented at faint absolute blue magnitudes ($M_B \geq -24$), an effect which cannot be explained by a potential LBQS selection bias against quasars which have large radio luminosities and small optical luminosities. The radio-loud (8 GHz luminosity $>10^{25}$ W Hz^{-1}) fraction is observed to change as a function of redshift and M_B, for $M_B < -24$, although the causal variable is ambiguous. The description most consistent with the available data is that radio-loud fraction is approximately constant over the range $-27.5 \lesssim M_B \lesssim -24$ and increases at brighter absolute magnitudes. The radio-loud fraction as a function of redshift reaches a local maximum at $z \approx 1$, and, aside from the effects of increased radio-loud fraction at bright M_B, remains roughly constant to redshifts approaching 5. The log $R_{8.4}$ distribution (radio-to-optical luminosity ratio) of the current LBQS sample may be bimodal, but the results of statistical tests are ambiguous, requiring a larger sample size to become definite.

Subject headings: quasars: general — radio continuum: galaxies — surveys

1. INTRODUCTION

A long-standing problem central to understanding the quasar phenomenon is the lack of a simple scaling between quasar radio and optical luminosity, the presence of which would result in a constant ratio of the luminosities in the two spectral regimes. The observed ratios of radio to optical luminosity, R, span several orders of magnitude. It is important to explain such a large spread, given that the radio and optical emission mechanisms are believed to be driven ultimately by the same central engine. The wide range of observed radio luminosity was once thought to arise from the orientation of a beamed relativistic jet (Scheuer & Readhead 1979), resulting in a spread in R if the optical emission is unbeamed or emitted in a jet with a different opening angle. However, a range in the luminosity of large-scale, nonbeamed radio emission indicates an intrinsic spread in radio power (Orr & Browne 1982). Coleman & Dopita (1992) hypothesized that quasar radio luminosity may depend on the angle of the accretion disk with respect to the rotation axis of the central supermassive black hole. The fundamental mechanism regulating radio emission may be connected in some way to the host galaxies of quasars, as is the case with radio galaxies and Seyfert galaxies. The results of some studies of quasar host galaxies are consistent with the stronger radio emitters residing in ellipticals and the radio-weak quasars existing in spirals, but these conclusions are not definitive (e.g., Smith et al. 1986; Véron-Cetty & Woltjer 1990).

Much of the basic data on the radio and optical properties of quasars has come from optical follow-up of radio surveys, such as the 3 CR (Spinrad et al. 1985), the 2 Jy survey of Wall & Peacock (1985), the 1 Jy survey (Kühr et al. 1981b), the S4 (Pauliny-Toth et al. 1978) and S5 (Kühr et al. 1981a) surveys to a limiting flux of 0.5 Jy, and the 100 mJy Parkes Selected Regions (Dunlop et al. 1989). Optically derived redshifts have enabled the determination of a quasar radio luminosity function and its evolution to redshifts $z > 3$ (Dunlop & Peacock 1990).

Since the initial realization that not all quasars are strong radio emitters (Sandage 1965), several optically selected quasar samples have been observed at radio frequencies (e.g., Sramek & Weedman 1980; Condon et al. 1981; Marshall 1987; Miller, Peacock, & Mead 1990, hereafter MPM). Typically only 10%–40% of the quasars were detected, even in relatively deep radio observations, and the radio luminosities of most of these detections lie below the luminosity range sampled by the radio surveys. The Very Large Array[1] (VLA) observations of the Palomer-Green (Schmidt & Green 1983) Bright Quasar Survey by Kellerman et al. (1989, hereafter PG), which detected more than 80% of the 114 quasars in the survey, are a notable exception to the low detection rates. The PG sample is consistent with two simple models of the joint optical and radio luminosity function, in which the radio luminosity function is either independent of optical luminosity or, as hypothesized by Schmidt (1970), is parameterized by R, i.e., a function of the ratio of radio to optical luminosity. MPM found that the R parameterization is inconsistent with the radio luminosities of quasars with faint absolute magnitudes.

Quasars have been designated either radio-loud or radio-quiet based on a division in R (e.g., PG) or radio luminosity, L (e.g., Peacock, Miller, & Longair 1986). Stocke et al. (1992)

[1] The Very Large Array (VLA) of the National Radio Astronomy Observatory is operated by Associated Universities, Inc., under a cooperative agreement with the National Science Foundation.

found statistical support for bimodal distributions in both log R and log L. Recently, La Franca et al. (1994) have analyzed the redshift and absolute magnitude dependence of the fraction of radio-loud quasars using a data set consisting of most of the available optically selected samples with radio observations. They determined that the radio-loud fraction is substantially higher for quasars with $z < 1$, a result due to the fact that the predominantly low redshift PG sample has a high overall radio-loud fraction; evolution is not required for $z > 1$ if the PG is excluded. The radio-loud fraction was found to be higher at bright absolute magnitudes, regardless of whether or not the PG sample was included in the analysis.

The Large Bright Quasar Survey (LBQS) (Hewett, Foltz, & Chaffee 1995) consists of more than 1050 quasars with magnitudes $16.0 \leq m_{B_J} \leq 18.85$ and redshifts $0.2 \leq z \leq 3.4$. Positions, magnitudes, redshifts, and spectra for the entire sample are now published (Hewett et al. 1995, and references therein). The LBQS was compiled using well-defined selection criteria, applied to objective-prism spectra of a broadband flux-limited catalog of objects. Quasar candidates were selected from among the objective-prism spectra according to a number of color and spectral feature-based criteria. The aim was to identify essentially all known types of quasars or active galactic nuclei whose broadband fluxes placed them within the magnitude limits of the LBQS.

Hewett et al. (1995) discuss the properties of the LBQS in some detail. The smooth number-redshift relation and high surface density of objects demonstrate that the LBQS is as effective as any existing optical survey of quasars. Direct comparison of the LBQS catalog with other surveys undertaken using a broad range of techniques shows that the only class of known active galactic nuclei to which the survey is not sensitive is featureless objects with red spectral energy distributions, e.g., some radio-selected BL Lac objects. Important advantages of the survey relative to other samples include (*a*) the very low percentage of objects that remain spectroscopically unidentified; only eight objects compared to the total of 1055 confirmed quasars (<1%) remain unclassified, and (*b*) the inclusion of quasars whose direct images are resolved due to the presence of an underlying galaxy. The very small percentage of candidates that remain unidentified ensures that bias against objects with weak emission lines is negligible, while the inclusion of objects with nonstellar morphology is important when the properties of quasars with low redshifts $z < 0.5$ are considered. The probability of selecting a candidate is a function of its intrinsic spectral energy distribution, a property common to all quasar surveys based on observed-frame, magnitude-limited samples (see Hewett & Foltz 1994). However, with the exception of red featureless active galactic nuclei (AGNs) and large amplitude photometrically variable objects such as optically violent variable quasars, the LBQS appears to be free of significant variations in the probability of detecting quasars whose magnitudes place them within the broadband flux limits.

The initial radio observations of the LBQS (Visnovsky et al. 1992, hereafter Paper I) consisted of 124 quasars in the redshift range $1.0 < z < 3.0$, chosen to complement the predominantly low redshift PG. The present work presents the radio data for an additional 132 LBQS quasars, which, together with the data from Paper I, span the full redshift range of the LBQS. The enlarged sample enables an independent and self-contained analysis of the evolution of the distribution of radio strength and its dependence on optical luminosity. Optical spectral properties, including broad absorption lines, of the LBQS radio sample are discussed in Francis, Hooper, & Impey (1993). Section 2 summarizes the observations and presents an analysis of the noise properties of the radio maps and the criteria for detection. Section 3 examines evidence for a bimodal distribution of radio strength and discusses evolution, correlation of radio strength with absolute magnitude, and potential selection effects. Section 4 summarizes the results. Details of a statistical test for a bimodal distribution and an examination of the impact of selection effects are presented in Appendices A and B, respectively.

2. OBSERVATIONS AND DATA REDUCTION

2.1. *Summary of Observations*

VLA observations at 8.4 GHz of 124 LBQS quasars in the redshift range $1.0 < z < 3.0$ were presented in Paper I. Subsequent observations at the same frequency of 132 additional LBQS quasars extended the redshift range to $0.2 < z < 3.4$. Table 1 summarizes each observing run, listing the date, number of quasars observed, VLA array configuration, pixel size of the maps, and the average angular extent of the major and minor axes of the beams at half-maximum intensity. All of the observations were snapshots, with exposure times ranging from 7.5 to 11 minutes. Table 2 lists the objects in the combined sample as follows.

Column (1): object name, listed in order of increasing right ascension.

Column (2): apparent B magnitude, calculated as described in § 2.3.

Column (3): redshift from Hewett et al. (1995).

Column (4): absolute B magnitude, calculated as described in § 2.3.

Column (5): flux density (mJy) at 8.4 GHz and 1 σ error, or 3 σ upper limit, measured as described in § 2.2.

Column (6): logarithm of the ratio of 8.4 GHz luminosity (W Hz^{-1}) to optical luminosity (W Hz^{-1}) averaged over the B passband; $R_{8.4} = L_{8.4}/L_B$. See § 2.3.

Column (7): logarithm of 8.4 GHz luminosity (W Hz^{-1}), log $L_{8.4}$. See § 2.3.

Standard AIPS software was employed to produce dirty total-intensity (Stokes I) maps for all fields. Those containing a strong source were subsequently CLEANed, with the exception of three previously catalogued sources: 1148−0007, a VLA calibrator; 1215+1121 (Bennett et al. 1986); and 1229−0207 (Kühr et al. 1981b). A noise analysis was performed on the VLA maps of the quasars listed in Paper I and the more recent sample of 132 objects. Quasars with measured radio flux above a preset multiple of the noise were considered to be detected, as described below.

TABLE 1

SUMMARY OF VLA OBSERVATIONS

Date	Number Observed	VLA Array Configuration	Pixel Size	FWHM Major[a]	FWHM Minor[b]
1989 May[c]....	97	B/C	0.″25	2.″5	0.″9
1989 Oct[c].....	27	C/D	0.25	5.8	2.9
1990 Oct.....	50	C	0.60	3.7	2.7
1991 Jan.....	82	C	0.60	4.5	2.5

[a] Average angular extent of the major axis of the beam profile at FWHM.
[b] Average angular extent of the minor axis of the beam profile at FWHM.
[c] These observations were also reported in Paper I.

TABLE 2

RADIO AND OPTICAL OBSERVATIONS OF LBQS QUASARS

Source (1)	B (2)	z (3)	M_B (4)	$S_{8.4}$ (mJy) (5)	$\log R_{8.4}$ (6)	$\log L_{8.4}$ ($\mathrm{WHz^{-1}}$) (7)
0006+0230	18.06	2.098	-27.11 ± 0.76	< 0.24	< 0.07	< 24.62
0006+0200	17.89	2.336	-27.39 ± 0.81	< 0.28	< 0.11	< 24.78
0009+0219	18.02	2.642	-27.69 ± 0.86	< 0.24	< 0.04	< 24.82
0013−0029	18.24	2.083	-26.92 ± 0.76	< 3.54	< 1.31	< 25.78
0018−0220	17.46	2.596	-28.19 ± 0.85	< 0.18	< -0.30	< 24.68
0019+0107	18.17	2.130	-27.03 ± 0.77	< 0.19	< 0.03	< 24.55
0025−0151	18.11	2.076	-27.03 ± 0.76	< 0.34	< 0.25	< 24.77
0027+0149	17.73	2.328	-27.55 ± 0.80	< 0.23	< -0.02	< 24.70
0028+0236	17.91	2.007	-27.17 ± 0.74	< 0.24	< 0.01	< 24.59
0040−2917	17.85	2.087	-27.31 ± 0.76	< 0.48	< 0.28	< 24.92
0041−2638	18.50	3.053	-27.88 ± 0.93	< 0.30	< 0.17	< 25.03
0041−2707	18.04	2.786	-27.89 ± 0.88	< 0.22	< -0.02	< 24.83
0041−2607	17.17	2.505	-28.35 ± 0.83	< 0.26	< -0.23	< 24.81
0041−2859	18.13	2.134	-27.08 ± 0.77	< 0.22	< 0.06	< 24.60
0042−2930	17.84	2.388	-27.51 ± 0.81	< 0.26	< 0.05	< 24.77
0045−3002	18.29	2.021	-26.80 ± 0.75	< 0.25	< 0.19	< 24.62
0047−2759	18.37	2.130	-26.83 ± 0.77	< 0.23	< 0.17	< 24.62
0048−2545	18.28	2.082	-26.88 ± 0.76	< 0.22	< 0.12	< 24.58
0049+0045	17.50	2.265	-27.70 ± 0.79	< 0.43	< 0.15	< 24.94
0050−2523	17.86	2.159	-27.38 ± 0.77	< 0.24	< -0.00	< 24.65
0052−0058	17.93	2.212	-27.24 ± 0.78	< 0.40	< 0.29	< 24.89
0053−0134	18.31	2.062	-26.82 ± 0.76	< 0.34	< 0.33	< 24.76
0100−3105	18.32	2.641	-27.39 ± 0.86	< 0.30	< 0.24	< 24.91
0105−2649	17.70	2.463	-27.75 ± 0.83	0.92 ± 0.07	0.53 ± 0.39	25.34 ± 0.21
0109+0213	17.66	2.343	-27.63 ± 0.81	0.31 ± 0.06	0.07 ± 0.39	24.83 ± 0.22
0252+0136	17.87	2.465	-27.58 ± 0.83	< 0.36	< 0.19	< 24.93
0254+0000	18.16	2.247	-27.03 ± 0.79	< 0.21	< 0.11	< 24.64
0256−0000	18.54	3.364	-28.43 ± 0.97	6.25 ± 0.19	1.34 ± 0.46	26.42 ± 0.25
0258+0210	17.99	2.524	-27.56 ± 0.84	< 1.47	< 0.83	< 25.56
0302−0019	18.13	3.281	-28.66 ± 0.96	0.63 ± 0.08	0.23 ± 0.46	25.41 ± 0.25
0307−0058	17.93	2.106	-27.25 ± 0.76	< 0.28	< 0.09	< 24.69
1009−0252	17.69	2.746	-28.18 ± 0.87	< 0.29	< -0.04	< 24.93
1010+0219	17.68	0.222	-22.83 ± 0.35	< 0.37	< 0.06	< 22.90
1011−0144	17.91	2.236	-27.27 ± 0.79	< 0.22	< 0.03	< 24.65
1013+0124	16.68	0.779	-26.44 ± 0.43	137.0 ± 5.6	2.26 ± 0.20	26.54 ± 0.10
1014+0023	18.22	2.291	-27.01 ± 0.80	< 0.26	< 0.21	< 24.73
1019+0147	17.36	0.791	-25.79 ± 0.44	< 0.29	< -0.13	< 23.88
1021−0250	17.44	0.496	-24.70 ± 0.37	< 0.29	< -0.09	< 23.49
1021−0118	17.93	0.743	-25.08 ± 0.44	< 0.29	< 0.09	< 23.83
1026−0144	17.13	0.217	-23.33 ± 0.34	< 0.32	< -0.22	< 22.81
1027−0114	17.62	0.958	-25.93 ± 0.49	< 0.32	< 0.01	< 24.09
1128+0022	18.02	1.379	-26.24 ± 0.60	< 0.23	< 0.06	< 24.26
1129−0218	17.43	1.247	-26.64 ± 0.57	< 0.22	< -0.21	< 24.15
1129−0229	17.74	0.333	-23.59 ± 0.36	< 0.23	< -0.09	< 23.05
1130+0018	18.20	1.255	-25.87 ± 0.58	< 0.31	< 0.25	< 24.31
1131−0039	17.91	0.268	-22.98 ± 0.36	< 0.40	< 0.18	< 23.09
1132−0302	17.01	0.237	-23.63 ± 0.34	< 0.40	< -0.17	< 22.98
1132−0054	18.11	2.753	-27.77 ± 0.88	< 0.21	< -0.01	< 24.79
1132−0013	17.77	0.955	-25.78 ± 0.49	< 0.52	< 0.28	< 24.30
1135+0044	17.52	0.803	-25.67 ± 0.45	< 0.30	< -0.05	< 23.92
1135−0255	18.30	2.407	-27.08 ± 0.82	< 0.27	< 0.24	< 24.78
1137+0110	18.24	1.138	-25.64 ± 0.55	70.19 ± 2.37	2.61 ± 0.25	26.57 ± 0.13
1138−0107	18.17	2.754	-27.72 ± 0.88	< 0.23	< 0.03	< 24.83
1138+0003	17.93	0.500	-24.23 ± 0.39	37.73 ± 0.81	2.20 ± 0.17	25.60 ± 0.07
1138+0204	17.64	0.383	-23.97 ± 0.36	< 5.14	< 1.20	< 24.50
1139−0257	18.09	1.028	-25.59 ± 0.52	< 0.22	< 0.05	< 24.00
1141−0222	18.09	1.394	-26.19 ± 0.61	< 0.19	< 0.01	< 24.20
1141+0227	17.72	0.216	-22.73 ± 0.36	< 0.24	< -0.10	< 22.69
1145−0039	18.14	1.941	-26.87 ± 0.73	< 0.22	< 0.06	< 24.52
1145−0216	17.78	0.566	-24.63 ± 0.40	< 0.73	< 0.43	< 23.99
1145+0235	17.92	1.217	-26.10 ± 0.56	0.27 ± 0.07	0.07 ± 0.29	24.22 ± 0.18
1146+0207	18.34	2.054	-26.79 ± 0.75	< 0.26	< 0.22	< 24.64

TABLE 2—*Continued*

Source (1)	B (2)	z (3)	M_B (4)	$S_{8.4}$ (mJy) (5)	$\log R_{8.4}$ (6)	$\log L_{8.4}$ (WHz^{-1}) (7)
1146−0128	16.67	0.460	−25.32 ± 0.36	< 0.40	< −0.26	< 23.56
1148−0007	17.29	1.976	−27.75 ± 0.73	1201 ± 27	3.46 ± 0.35	28.27 ± 0.18
1148−0033	17.76	0.800	−25.42 ± 0.45	4.14 ± 0.12	1.17 ± 0.21	25.04 ± 0.10
1148+0055	18.19	1.885	−26.75 ± 0.72	< 0.25	< 0.14	< 24.55
1149+0043	17.07	0.466	−24.94 ± 0.36	< 0.49	< −0.02	< 23.66
1150+0127	17.80	1.636	−26.82 ± 0.66	< 0.20	< −0.08	< 24.35
1150+0041	17.65	0.781	−25.47 ± 0.45	< 0.28	< −0.03	< 23.86
1203+1043	17.96	1.333	−26.23 ± 0.60	< 0.45	< 0.31	< 24.51
1204+0935	17.88	1.559	−26.63 ± 0.65	< 0.23	< 0.00	< 24.36
1204+1136	18.08	1.010	−25.58 ± 0.52	< 0.38	< 0.27	< 24.21
1205+1729	17.12	0.548	−25.22 ± 0.40	< 0.30	< −0.20	< 23.59
1206+1318	17.94	1.334	−26.26 ± 0.60	< 0.21	< −0.01	< 24.19
1206+1500	18.07	2.595	−27.58 ± 0.85	< 0.33	< 0.20	< 24.94
1206+1716	18.13	1.012	−25.53 ± 0.52	< 0.35	< 0.26	< 24.18
1208+1250	16.88	1.002	−26.75 ± 0.50	0.26 ± 0.07	−0.36 ± 0.26	24.04 ± 0.16
1208+1535	17.97	1.961	−27.06 ± 0.74	< 0.20	< −0.02	< 24.50
1209+1046	17.73	2.187	−27.54 ± 0.78	< 0.48	< 0.24	< 24.96
1209+1524	18.50	3.059	−27.88 ± 0.93	< 0.34	< 0.22	< 25.09
1210+1731	17.44	2.543	−28.14 ± 0.84	< 0.24	< −0.16	< 24.79
1210+1507	17.29	1.613	−27.29 ± 0.66	0.23 ± 0.073	−0.23 ± 0.34	24.39 ± 0.21
1210+1425	17.95	0.723	−24.99 ± 0.45	< 0.21	< −0.03	< 23.67
1210+1324	17.62	1.141	−26.27 ± 0.55	429.8 ± 4.9	3.14 ± 0.25	27.36 ± 0.13
1211+0848	17.87	0.810	−25.33 ± 0.47	7.06 ± 0.15	1.44 ± 0.21	25.29 ± 0.10
1211+1106	17.73	1.337	−26.47 ± 0.60	< 0.38	< 0.14	< 24.44
1211+0841	17.65	0.585	−24.83 ± 0.41	< 0.96	< 0.50	< 24.14
1212+1445	17.94	1.656	−26.70 ± 0.67	0.45 ± 0.07	0.31 ± 0.32	24.70 ± 0.18
1212+0830	18.12	1.664	−26.53 ± 0.67	< 0.29	< 0.19	< 24.51
1212+1045	17.79	1.970	−27.25 ± 0.74	< 0.34	< 0.12	< 24.73
1212+0854	18.22	2.344	−27.07 ± 0.81	< 0.67	< 0.62	< 25.16
1212+1411	18.03	0.847	−25.27 ± 0.48	< 0.25	< 0.07	< 23.89
1213+1015	18.28	2.513	−27.25 ± 0.84	< 0.34	< 0.31	< 24.92
1213+0922	18.15	2.714	−27.67 ± 0.87	30.61 ± 1.13	2.16 ± 0.41	26.94 ± 0.22
1213+1208	17.31	1.486	−27.09 ± 0.63	< 0.41	< 0.03	< 24.57
1213+1722	18.08	1.205	−25.91 ± 0.57	< 0.35	< 0.25	< 24.33
1213+1709	17.75	1.196	−26.23 ± 0.56	< 0.21	< −0.10	< 24.09
1214+1804	16.73	0.374	−24.84 ± 0.36	< 0.31	< −0.36	< 23.27
1214+1753	17.68	0.679	−25.12 ± 0.43	< 0.21	< −0.12	< 23.62
1214+0826	17.30	0.343	−24.09 ± 0.37	< 0.26	< −0.22	< 23.12
1215+1202	18.28	2.841	−27.73 ± 0.89	< 0.23	< 0.06	< 24.86
1215+1121	16.62	1.398	−27.66 ± 0.60	133.9 ± 6.6	2.25 ± 0.28	27.03 ± 0.15
1216+1754	18.13	1.810	−26.72 ± 0.71	49.76 ± 2.62	2.42 ± 0.33	26.81 ± 0.18
1216+1032	17.62	0.542	−24.70 ± 0.40	< 0.31	< 0.00	< 23.58
1216+1656	18.26	2.818	−27.72 ± 0.89	< 0.25	< 0.09	< 24.89
1218+1611	17.78	0.231	−22.81 ± 0.38	< 0.21	< −0.13	< 22.69
1220+0939	17.62	0.681	−25.18 ± 0.43	0.50 ± 0.11	0.21 ± 0.22	23.99 ± 0.13
1222+1640	17.78	0.549	−24.57 ± 0.41	< 0.25	< −0.02	< 23.50
1222+1433	17.02	1.337	−27.18 ± 0.59	< 0.24	< −0.33	< 24.25
1222+1235	17.45	0.412	−24.31 ± 0.38	21.80 ± 0.43	1.76 ± 0.16	25.19 ± 0.06
1222+0901	17.89	0.535	−24.40 ± 0.41	< 0.28	< 0.07	< 23.54
1222+1334	17.99	1.796	−26.84 ± 0.70	< 0.20	< −0.02	< 24.42
1223+1723	18.14	2.402	−27.23 ± 0.82	< 0.47	< 0.42	< 25.03
1224+1244	18.39	2.156	−26.84 ± 0.78	< 0.44	< 0.46	< 24.91
1224+1538	18.05	1.771	−26.75 ± 0.70	< 0.23	< 0.07	< 24.48
1225+1502	17.88	0.856	−25.45 ± 0.48	< 0.24	< −0.01	< 23.87
1225+0836	17.85	1.471	−26.53 ± 0.63	< 0.35	< 0.17	< 24.49
1225+1512	18.10	1.990	−26.96 ± 0.74	< 0.23	< 0.08	< 24.57
1226+1526	18.22	1.122	−25.63 ± 0.55	< 0.28	< 0.21	< 24.17
1228+1642	17.59	0.841	−25.70 ± 0.47	< 0.31	< −0.01	< 23.97
1228+1116	17.42	0.237	−23.22 ± 0.37	< 0.39	< −0.02	< 22.97
1228+1808	18.17	2.649	−27.55 ± 0.86	< 0.32	< 0.21	< 24.94
1228+1216	17.55	1.408	−26.74 ± 0.61	< 0.55	< 0.25	< 24.65
1228+1602	17.76	0.511	−24.45 ± 0.40	< 0.28	< 0.00	< 23.49

TABLE 2—*Continued*

Source (1)	B (2)	z (3)	M_B (4)	$S_{8.4}$ (mJy) (5)	$\log R_{8.4}$ (6)	$\log L_{8.4}$ ($\mathrm{WHz^{-1}}$) (7)
1229+1133	18.39	1.028	−25.29 ± 0.53	< 0.32	< 0.32	< 24.14
1229−0207	17.69	1.045	−26.03 ± 0.52	283.9 ± 23.9	2.99 ± 0.24	27.11 ± 0.12
1229+0106	18.02	0.477	−24.04 ± 0.40	< 0.26	< 0.08	< 23.41
1229+1250	17.95	1.246	−26.12 ± 0.58	< 0.32	< 0.15	< 24.31
1230+1042	18.37	2.420	−27.03 ± 0.82	< 0.33	< 0.36	< 24.88
1230+1430	17.67	0.332	−23.66 ± 0.38	< 0.35	< 0.04	< 23.21
1230−0015	17.03	0.470	−25.00 ± 0.38	63.33 ± 1.91	2.06 ± 0.16	25.77 ± 0.06
1230+1627B	17.79	2.700	−28.02 ± 0.87	< 0.24	< −0.07	< 24.84
1230+1052	17.64	1.377	−26.62 ± 0.60	< 0.26	< −0.03	< 24.31
1230+0947	16.17	0.415	−25.61 ± 0.35	< 0.30	< −0.59	< 23.35
1231+0816	18.30	1.510	−26.13 ± 0.64	< 0.25	< 0.21	< 24.38
1231+0813	18.09	1.190	−25.89 ± 0.56	< 0.26	< 0.13	< 24.19
1233+1524	18.11	1.544	−26.38 ± 0.65	< 0.26	< 0.14	< 24.40
1234−0209	17.80	1.620	−26.79 ± 0.66	< 0.34	< 0.14	< 24.56
1234+0122	18.04	2.025	−27.05 ± 0.75	< 1.06	< 0.71	< 25.24
1235+0857	18.32	2.898	−27.79 ± 0.90	0.41 ± 0.08	0.29 ± 0.44	25.12 ± 0.25
1235+0216	17.68	0.672	−25.09 ± 0.43	< 0.20	< −0.16	< 23.58
1235+1807B	16.89	0.449	−25.05 ± 0.37	1.68 ± 0.26	0.43 ± 0.17	24.16 ± 0.09
1236+1543	17.64	0.315	−23.58 ± 0.37	< 0.31	< −0.01	< 23.12
1236+1308	18.14	1.303	−26.01 ± 0.59	< 0.26	< 0.15	< 24.26
1236+0128	17.66	1.262	−26.43 ± 0.58	< 0.43	< 0.17	< 24.45
1236+0903	17.58	0.498	−24.57 ± 0.39	< 0.39	< 0.08	< 23.62
1236+1103	17.85	1.304	−26.30 ± 0.59	< 0.28	< 0.07	< 24.29
1236−0207	18.21	2.244	−26.98 ± 0.79	< 0.32	< 0.30	< 24.80
1237+1752	17.63	0.913	−25.82 ± 0.49	< 0.31	< 0.00	< 24.04
1237+0834	18.25	1.075	−25.52 ± 0.54	< 0.23	< 0.14	< 24.06
1237+1042	18.23	1.030	−25.46 ± 0.53	< 0.23	< 0.12	< 24.01
1237+1325	17.95	1.727	−26.79 ± 0.69	< 0.28	< 0.11	< 24.53
1237+0950	17.93	0.736	−25.05 ± 0.45	< 0.30	< 0.10	< 23.83
1237+0204	17.53	0.665	−25.22 ± 0.43	< 0.37	< 0.05	< 23.84
1238+1006	18.11	1.046	−25.61 ± 0.53	< 0.22	< 0.06	< 24.01
1238+0039	18.24	1.361	−26.00 ± 0.61	< 0.35	< 0.32	< 24.43
1238+1013	18.21	1.184	−25.76 ± 0.56	< 0.20	< 0.07	< 24.08
1239−0231	17.75	1.234	−26.30 ± 0.57	< 0.32	< 0.07	< 24.30
1239+0028	17.49	1.214	−26.52 ± 0.56	0.38 ± 0.09	0.05 ± 0.28	24.37 ± 0.17
1239+1435	17.91	1.948	−27.11 ± 0.73	< 0.33	< 0.15	< 24.71
1239+1118	18.13	1.487	−26.27 ± 0.63	0.47 ± 0.11	0.41 ± 0.31	24.63 ± 0.18
1240+1754	17.44	0.458	−24.54 ± 0.38	< 0.33	< −0.05	< 23.47
1240+0224	17.98	0.790	−25.16 ± 0.46	7.19 ± 0.16	1.50 ± 0.21	25.27 ± 0.10
1240+1504	18.02	1.861	−26.89 ± 0.71	< 0.22	< 0.02	< 24.49
1241+1228	17.86	0.320	−23.39 ± 0.38	< 0.27	< 0.01	< 23.08
1242−0123	17.36	0.491	−24.76 ± 0.39	< 0.28	< −0.14	< 23.47
1242+1749	17.70	0.264	−23.16 ± 0.37	< 0.30	< −0.02	< 22.95
1242+0006	17.78	2.075	−27.37 ± 0.76	< 0.31	< 0.06	< 24.72
1242+1737	17.85	1.863	−27.06 ± 0.71	< 0.21	< −0.04	< 24.48
1243+1456	17.63	0.582	−24.84 ± 0.41	< 0.36	< 0.08	< 23.72
1243−0011	18.26	1.683	−26.42 ± 0.68	< 0.33	< 0.30	< 24.58
1243+1701	17.64	0.459	−24.34 ± 0.39	< 0.28	< −0.03	< 23.41
1244+1703	17.53	1.588	−27.02 ± 0.65	< 0.22	< −0.14	< 24.37
1244+0240	17.94	0.934	−25.57 ± 0.50	< 0.26	< 0.04	< 23.98
1244+1329	17.10	0.512	−25.11 ± 0.38	< 0.39	< −0.10	< 23.64
1244−0126	17.58	0.346	−23.83 ± 0.37	< 0.30	< −0.04	< 23.19
1245+1719	17.79	0.752	−25.25 ± 0.45	< 0.29	< 0.03	< 23.84
1246−0059	17.90	2.442	−27.53 ± 0.83	< 0.29	< 0.11	< 24.83
1246+0032	18.16	2.305	−27.08 ± 0.80	< 0.35	< 0.32	< 24.87
1246−0217	18.14	2.106	−27.04 ± 0.76	< 0.25	< 0.12	< 24.64
1247−0213	18.05	1.313	−26.11 ± 0.59	< 0.30	< 0.17	< 24.33
1308−0104	18.10	2.584	−27.53 ± 0.85	< 0.30	< 0.16	< 24.89
1308+0109	18.11	1.075	−25.66 ± 0.52	32.93 ± 0.72	2.22 ± 0.24	26.19 ± 0.12
1311+0217	16.99	0.306	−24.17 ± 0.31	< 0.45	< −0.11	< 23.25
1313+0111	18.28	1.569	−26.24 ± 0.64	< 0.35	< 0.34	< 24.54
1313−0138	17.72	0.406	−24.00 ± 0.34	< 0.41	< 0.15	< 23.47

TABLE 2—*Continued*

Source (1)	B (2)	z (3)	M_B (4)	$S_{8.4}$ (mJy) (5)	$\log R_{8.4}$ (6)	$\log L_{8.4}$ (WHz^{-1}) (7)
1313+0107	18.16	2.393	−27.20 ± 0.81	3.91 ± 0.11	1.35 ± 0.39	25.94 ± 0.21
1314−0008	18.22	1.747	−26.55 ± 0.68	< 0.31	< 0.26	< 24.59
1315+0127	17.93	1.628	−26.68 ± 0.66	< 0.29	< 0.12	< 24.50
1315+0140	17.99	0.689	−24.84 ± 0.42	0.34 ± 0.08	0.19 ± 0.22	23.83 ± 0.14
1316+0023	17.91	0.492	−24.22 ± 0.37	< 0.26	< 0.04	< 23.44
1317−0142	17.26	0.225	−23.27 ± 0.31	0.41 ± 0.11	−0.06 ± 0.17	22.95 ± 0.12
1317−0018	17.76	0.354	−23.69 ± 0.34	< 0.23	< −0.07	< 23.10
1319+0039	17.95	1.619	−26.64 ± 0.65	53.29 ± 1.07	2.38 ± 0.31	26.75 ± 0.16
1319+0033	18.01	0.530	−24.26 ± 0.38	< 0.40	< 0.27	< 23.68
1320+0048	18.25	1.954	−26.78 ± 0.73	< 0.31	< 0.26	< 24.68
1320−0006	18.22	1.388	−26.05 ± 0.60	< 0.35	< 0.31	< 24.44
1320+0103	18.15	1.776	−26.66 ± 0.69	0.33 ± 0.08	0.26 ± 0.34	24.63 ± 0.20
1321−0145	17.71	0.224	−22.81 ± 0.32	< 0.27	< −0.06	< 22.77
1323−0248	17.44	2.120	−27.76 ± 0.76	15.96 ± 0.29	1.64 ± 0.36	26.45 ± 0.19
1324+0039	18.26	1.061	−25.48 ± 0.52	53.99 ± 1.80	2.50 ± 0.24	26.40 ± 0.12
1326+0206	17.35	1.416	−26.95 ± 0.60	< 0.39	< 0.02	< 24.51
1329+0242	17.82	1.583	−26.72 ± 0.65	< 0.24	< 0.00	< 24.40
1329+0018	18.24	2.351	−27.07 ± 0.81	< 0.31	< 0.30	< 24.83
1330+0113	18.13	1.511	−26.30 ± 0.63	< 0.24	< 0.12	< 24.35
1331−0108	17.92	1.881	−27.02 ± 0.71	0.68 ± 0.08	0.47 ± 0.34	24.99 ± 0.19
1332−0045	17.44	0.672	−25.33 ± 0.41	< 0.33	< −0.03	< 23.80
1333+0133	17.95	1.577	−26.59 ± 0.65	0.26 ± 0.08	0.07 ± 0.33	24.42 ± 0.21
1334−0033	17.52	2.801	−28.43 ± 0.88	0.20 ± 0.06	−0.29 ± 0.44	24.78 ± 0.27
1334+0212	17.85	2.382	−27.50 ± 0.81	< 0.30	< 0.11	< 24.82
1334−0232	17.66	0.722	−25.28 ± 0.43	< 0.40	< 0.13	< 23.95
1337−0146	17.54	1.014	−26.12 ± 0.51	< 0.24	< −0.13	< 24.01
1338−0030	17.25	0.385	−24.37 ± 0.35	< 0.30	< −0.17	< 23.28
1340−0038	16.98	0.326	−24.31 ± 0.33	< 0.17	< −0.52	< 22.90
1340+0107	18.15	1.067	−25.61 ± 0.52	< 0.26	< 0.13	< 24.09
1342−0000	17.77	0.244	−22.93 ± 0.35	< 0.26	< −0.05	< 22.82
1343−0221	17.99	0.509	−24.21 ± 0.38	0.72 ± 0.21	0.51 ± 0.21	23.90 ± 0.14
1344+0137	17.42	1.913	−27.56 ± 0.72	< 0.27	< −0.12	< 24.61
1344−0105	17.70	1.737	−27.05 ± 0.68	< 0.26	< −0.02	< 24.50
1345−0137	18.30	1.929	−26.70 ± 0.73	< 0.33	< 0.30	< 24.69
1346+0007	18.16	1.128	−25.70 ± 0.54	< 0.23	< 0.10	< 24.09
1346−0251	17.75	1.715	−26.97 ± 0.68	< 0.27	< 0.01	< 24.51
1347−0026	17.68	0.515	−24.54 ± 0.38	< 0.33	< 0.04	< 23.57
1348−0054	18.15	1.474	−26.23 ± 0.63	< 0.30	< 0.23	< 24.43
1348+0118	17.09	1.089	−26.71 ± 0.52	< 0.28	< −0.25	< 24.14
1349+0057	17.71	1.144	−26.18 ± 0.54	< 0.29	< 0.01	< 24.20
1428+0202	17.90	2.106	−27.28 ± 0.76	< 0.24	< 0.00	< 24.62
1429−0100	17.06	0.659	−25.67 ± 0.41	< 0.44	< −0.06	< 23.91
1429−0036	17.80	1.180	−26.16 ± 0.56	< 0.76	< 0.47	< 24.64
1429+0127	18.14	1.092	−25.66 ± 0.54	< 0.26	< 0.13	< 24.11
1429−0053	17.74	2.078	−27.41 ± 0.76	< 1.15	< 0.62	< 25.29
1429+0137	17.80	1.533	−26.67 ± 0.64	< 0.27	< 0.03	< 24.41
1430−0046	17.79	1.023	−25.88 ± 0.52	14.97 ± 0.31	1.75 ± 0.24	25.81 ± 0.12
1430−0041	16.40	1.116	−27.44 ± 0.53	0.27 ± 0.09	−0.53 ± 0.28	24.15 ± 0.19
1433+0223	18.27	2.140	−26.95 ± 0.77	< 0.83	< 0.69	< 25.17
1435−0134	16.01	1.310	−28.15 ± 0.57	67.75 ± 0.98	1.71 ± 0.27	26.68 ± 0.14
1435+0228	18.16	1.676	−26.51 ± 0.68	< 0.25	< 0.15	< 24.46
1437+0224	17.66	0.821	−25.57 ± 0.46	< 0.31	< 0.01	< 23.95
1438+0002	17.84	1.446	−26.50 ± 0.62	< 0.32	< 0.12	< 24.43
1440+0149	18.20	1.169	−25.74 ± 0.56	< 0.46	< 0.41	< 24.42
1440−0024	17.88	1.815	−26.97 ± 0.70	< 0.24	< 0.01	< 24.51
1440+0154	17.18	1.359	−27.05 ± 0.60	< 0.27	< −0.21	< 24.31
1440−0234	17.30	0.678	−25.49 ± 0.42	< 0.26	< −0.19	< 23.71
1441+0142	17.19	0.296	−23.91 ± 0.36	< 0.29	< −0.22	< 23.04
1442−0011	18.24	2.226	−26.94 ± 0.79	< 0.41	< 0.42	< 24.90
1443+0141	18.22	2.451	−27.21 ± 0.83	0.49 ± 0.14	0.47 ± 0.41	25.06 ± 0.25
1445−0231	18.09	1.734	−26.66 ± 0.69	< 0.23	< 0.07	< 24.44
2206−1958A	17.56	2.558	−28.04 ± 0.85	< 0.27	< −0.08	< 24.84
2209−1842	17.74	2.092	−27.42 ± 0.76	< 0.25	< −0.03	< 24.63
2212−1759	17.94	2.217	−27.23 ± 0.79	< 0.27	< 0.12	< 24.72
2230+0232	18.14	2.147	−27.08 ± 0.77	< 0.35	< 0.27	< 24.81
2231−0015	17.74	3.015	−28.57 ± 0.92	0.51 ± 0.09	0.11 ± 0.44	25.25 ± 0.25
2241+0014	17.65	2.131	−27.55 ± 0.76	< 0.20	< −0.16	< 24.56
2243+0141	18.26	2.314	−26.99 ± 0.80	< 0.23	< 0.18	< 24.69
2244−0105	17.99	2.030	−27.11 ± 0.75	< 0.26	< 0.09	< 24.64
2248+0127	18.23	2.559	−27.37 ± 0.85	< 0.26	< 0.17	< 24.83

2.2. *Noise Analysis and Source Detection*

A procedure was developed in Paper I to fit the core of each beam to various regions of the associated map. The core is chosen to extend to approximately the first minimum of the beam profile. To fit this core to a region centered on an arbitrary pixel in the map, the beam is translated without rotation to the desired location, and a least-squares fit is performed by minimizing

$$X = \sum_{i=1}^{n} (m_i - fb_i)^2 , \quad (1)$$

where m_i and b_i are the intensity values of the ith pixel in the overlap of the map and the beam core, respectively. The number of pixels in the fitted region is n, and f is a scale factor for the beam, which is adjusted to minimize the value of X. The value of f at a minimum X is the flux in Jy assigned to the map pixel, since the beam represents the intensity distribution of a 1 Jy point source.

The noise estimate for maps without strong sources was obtained by performing the fitting routine on pixels randomly distributed across the map. The number of random points was chosen to keep the coincidence rate $\lesssim 5\%$.

All but a few of the maps produced noise distributions which closely approximated a Gaussian with a mean of zero. The cumulative distributions of fluxes from the random sampling of apparently empty maps indicate that the probability of obtaining a 3 σ or greater positive fluctuation is 1.8 times greater than the value expected for a Gaussian noise model: $1.8(1.35 \times 10^{-3}) = 2.4 \times 10^{-3}$. The excess of positive fluctuations may be due to weak sources in the maps, or it may be due to part of the sidelobe patterns from unknown off-map sources. A few of the nondetections have 3 σ upper limits much higher than the typical values (see Table 2). Most of these high limits are due to observed nearby strong sources.

The beam was fitted to each pixel whose center was within 2″ of the center of the map to determine whether a source is present, and, if so, to measure its position. If the maximum flux assigned to any pixel within this area, $f_{\max}$, equaled or exceeded 3 times the rms noise of the map (3 σ), then a detection of $f_{\max}$ Jy was adopted for the object. Table 2 contains the results of this analysis for both the sample from Paper I and the new observations: fluxes with 1 σ noise values for 44 detections and 3 σ upper limits for the remaining quasars. The pointing accuracy of the VLA is generally much better than the astrometric accuracy of the LBQS; the latter is estimated to be $\lesssim 2''$ for the original quasar positions (Morris et al. 1991, and references therein), which were the coordinates used in the VLA observations. An internal consistency check of the positional accuracy was performed by analyzing the data using a 4.″5 search radius. Every strong source ($f_{\max} > 7$ σ) discovered in this test, with the exception of one, lay within 2″ of the map center. The exception, 1229−0207, is located $\approx 8''$ from the center of the map. Since the LBQS coordinates differ by less than 3″ from the position of a VLBI source (Wehrle, Morabito, & Preston 1984), it is assumed that the VLA was misaligned and the radio source is associated with the quasar. It is possible that the VLA was mispointed for other LBQS quasars with detectable radio flux, which would be difficult to determine if the radio source were faint or displaced by a large angle from the center of the map. There is a noticeable source within 1′ of the map center for three quasars listed as upper limits in Table 2: 0049+0045, 1429−0036, and 2244−0105, located 26″, 47″, and 29″, respectively, from the map center.

The number of independent sampling points within the search region of each map was approximated by the ratio of the area of the 2″ search disk to the area of the beam at half-maximum. Table 1 lists the average FWHM of the beam major and minor axes. When this area ratio was less than 1, the number of independent points was assumed to be 1. The average of the number of independent sample points per search disk for all of the maps in the snapshot survey is 3.9. The expected total number of spurious 3 σ or greater detections is the product of the total number of objects, the probability of a spurious source, and the number of independent sample points per search region; $256(2.4 \times 10^{-3})(3.9) \approx 2.4$.

The detection method is optimized for point sources. Given the resolution of the maps (Table 1) and the redshifts of the quasars, hot spots in jets and the gross features of extended emission are expected to be the only structures present in these maps, in addition to the core sources. Only seven of the 44 detections have noticeable multiple structure, and all of these are core-dominated, with flux from other features amounting to no more than 50% of the core flux. Table 2 lists only the detections of, and upper limits to, the unresolved core fluxes of the quasars.

There are discrepancies between Table 2 and seven quasars listed in Paper I. The flux density for 1229−0207 listed in Paper I was measured at the center of the map, but, as noted above, the radio source is offset by 8″, and the flux density measured at the position of the source is listed in Table 2. Slight changes in the noise analysis technique from Paper I resulted in the reclassification of a nondetection to a detection (1334−0033) and a detection to a nondetection (1237+1325). Upper limits instead of detected flux were listed for 1239+1118, 1320+0103, and 1333+0133 in Paper I due to typographical errors. A detection was listed for 1203+1043 in Paper I based on analysis of a CLEANed map which contained no obvious radio source. However, the quasar was not detected in the unCLEANed map; consequently it is listed as an upper limit in Table 2. All of the detections which were added or deleted have flux densities near the 3 σ detection limit.

2.3. *Derived Quantities*

The optical magnitudes measured for objects in the LBQS are total B_J magnitudes, containing contributions from the quasar nucleus and any host galaxy. The B_J band is the natural system of the Kodak IIIa-J emulsion and GG 395 filter. Apparent B_J magnitudes of quasars with redshifts $z < 2.2$ were converted to rest-frame absolute Johnson B magnitudes (M_B) using k-corrections calculated from a composite LBQS spectral energy distribution (Francis et al. 1991). Since the B and B_J passbands can include Lyman α absorption systems for $z > 2.2$, the high redshift k-corrections were calculated (S. J. Warren 1994, private communication) using the mean Lyman α absorption as a function of wavelength and redshift from the model of Møller & Warren (1991) with parameters as given in Warren, Hewett, & Osmer (1994). A power-law continuum ($f_\nu \propto \nu^\alpha$; $\alpha = -0.75$) and Lyα/N v emission lines of 84 Å rest-frame equivalent width replaced the LBQS composite spectrum shortward of $\lambda = 1290$ Å. The conversion from B_J to Johnson B as a function of redshift is

$$(B - B_J)_{\text{observed}} = m_B - m_{B_J} = M_B - M_{B_J} + \Delta_{B-B_J} k(z) , \quad (2)$$

$$(B - B_J)_{\text{observed}} = -2.5[\log \bar{F}_B(\lambda) - \log \bar{F}_{B_J}(\lambda)] + \Delta_{B-B_J} k(z) + C , \quad (3)$$

where $\bar{F}_B(\lambda)$ and $\bar{F}_{B_J}(\lambda)$ are the flux densities of the LBQS composite spectrum averaged over the rest-frame B and B_J passbands, respectively, $\Delta_{B-B_J}k(z)$ is the difference in k-corrections between B and B_J, and C is a constant depending only on the zero-point flux densities of the two passbands. The final expression for the conversion is

$$(B-B_J)_{\rm observed} = \Delta_{B-B_J}k(z) + 0.04\ . \quad (4)$$

Rest-frame absolute magnitudes and 8.4 GHz luminosities ($L_{8.4}$) were calculated assuming $H_0 = 50$ km s^{-1} Mpc^{-1}, $q_0 = 0.5$, a radio spectral index $\alpha = -0.5$ ($f_\nu \propto \nu^\alpha$), and the optical k-corrections described above. The derived quantities M_B, $L_{8.4}$, and $R_{8.4}$, the ratio of $L_{8.4}$ to the average optical luminosity over the B passband, are listed in columns (4), (7), and (6), respectively, of Table 2.

Errors in log $L_{8.4}$ and M_B are due to measurement uncertainty, a dispersion in k-corrections, and source variability. Uncertainty in the measured radio flux values, along with an uncertainty in the 4.8–14.5 GHz spectral index of $\approx$0.4 (Aller, Aller, & Hughes 1992), lead to the error in the derived value of log $L_{8.4}$ listed in Table 2 for each detection. Photometric imprecision in the LBQS B_J magnitudes is $\approx$0.15 mag (Hewett et al. 1995). The LBQS survey plates predate the VLA observations by 3–14 yr, which introduces an additional uncertainty due to variability of the quasars (e.g., Hawkins 1986). Variability uncertainties as a function of the difference in epoch between the optical and radio observations were calculated for each quasar in the sample using equation (20) of Hook et al. (1994). These magnitude uncertainties were combined in quadrature with a rather large assumed uncertainty due to a dispersion in rest-frame optical to near-UV spectral index of $\approx$0.6 among LBQS quasars (Francis 1993), resulting in the errors in M_B listed for each object in Table 2. Errors in log $R_{8.4}$ for the detections are the quadrature sum of uncertainties in M_B and $L_{8.4}$.

3. RADIO AND OPTICAL PROPERTIES

3.1. *The Subsample of the LBQS with Radio Measurements*

The apparent magnitude range of the LBQS is constrained to $16.0 \le B_J \le 18.85$ (Hewett et al. 1995). The VLA sample was chosen to span the entire redshift range of the LBQS, but it excluded quasars with apparent magnitudes near the faint limit of the survey. These criteria are reflected in cumulative distributions of apparent and absolute magnitude and redshift for the radio sample and the LBQS quasars not observed at the VLA (Fig. 1). The cumulative distributions of the same properties for radio detections and nondetections within the VLA sample are compared in Figure 2. Kolmogorov-Smirnov (KS) tests on each pair of distributions in Figure 2 indicate that LBQS quasars with detectable radio fluxes have a marginally significantly different absolute magnitude distribution but are not found at significantly different redshifts than those which were not detected. The KS probability that the M_B, z, and B distribution pairs are drawn from the same parent population is 10%, 82%, and 29%, respectively. Figure 3 shows absolute magnitude plotted against redshift for the radio detections (*filled circles*), nondetections (*crosses*), and, for clarity, $\frac{1}{3}$ of the LBQS quasars without radio observations (Y-shaped symbol), selected without regard to redshift or absolute magnitude. The bias toward bright magnitudes in the radio sample is apparent, as is the strong correlation between M_B and redshift, which is responsible for the well-known difficulties in disentangling redshift evolution of radio properties from changes with optical luminosity in all flux-limited quasar samples of limited dynamic range.

3.2. *The Relationship between Radio and Optical Luminosity*

The distributions of log $R_{8.4}$ and log $L_{8.4}$ are plotted against M_B in Figure 4. There are no detections in the range $0.54 <$ log $R_{8.4} < 1.17$ for all values of M_B (Fig. 4*a*), which suggests a bimodal distribution. The luminosity of the corresponding division in the log $L_{8.4}$ distribution increases with M_B (Fig. 4*b*) from log $L_{8.4} \approx 24$ at $M_B = -24$ to log $L_{8.4} \approx 26$ at $M_B = -28$.

3.2.1. *Evidence for a Bimodal Distribution of* log $R_{8.4}$

The possible presence of a bimodal distribution in log $R_{8.4}$ for the LBQS radio sample was tested quantitatively with the Lee statistic (Lee 1979; Fitchett 1988). For two-dimensional data (M_B and log $R_{8.4}$ in the present case) the statistic is based on the clumpiness in the projection of the data points onto a line. The projected data with the maximum amount of clumping, determined by rotating the line, is tested for consistency with a bimodal distribution. Specifically, for each orientation of the projection line, a measure of the scatter of the data is calculated from the distances between the points along the line.

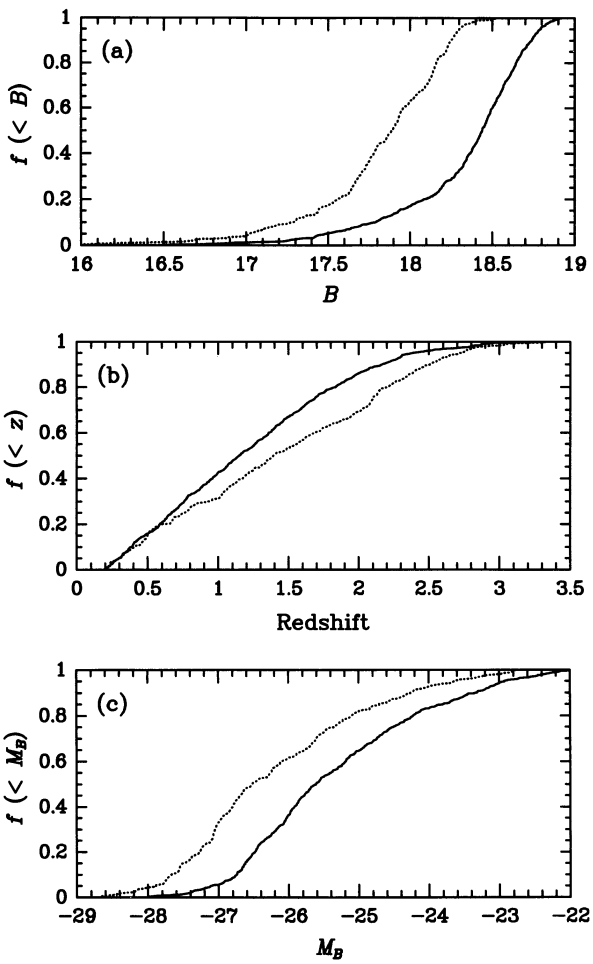

FIG. 1.—Cumulative distributions of (*a*) Johnson B magnitude, (*b*) redshift, and (*c*) M_B for the LBQS radio sample (*dotted line*) and the LBQS quasars not observed at the VLA (*solid line*).

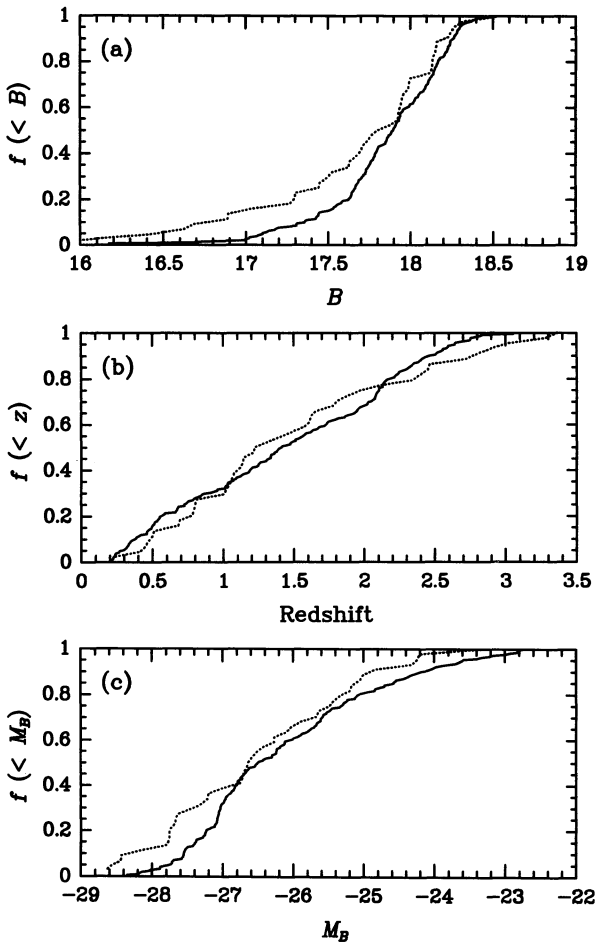

FIG. 2.—Cumulative distributions of (*a*) Johnson *B* magnitude, (*b*) redshift, and (*c*) M_B within the subsample of the LBQS observed in the radio. The dotted line in each panel indicates the radio detections (44 objects), and the solid line represents the nondetections (212 objects).

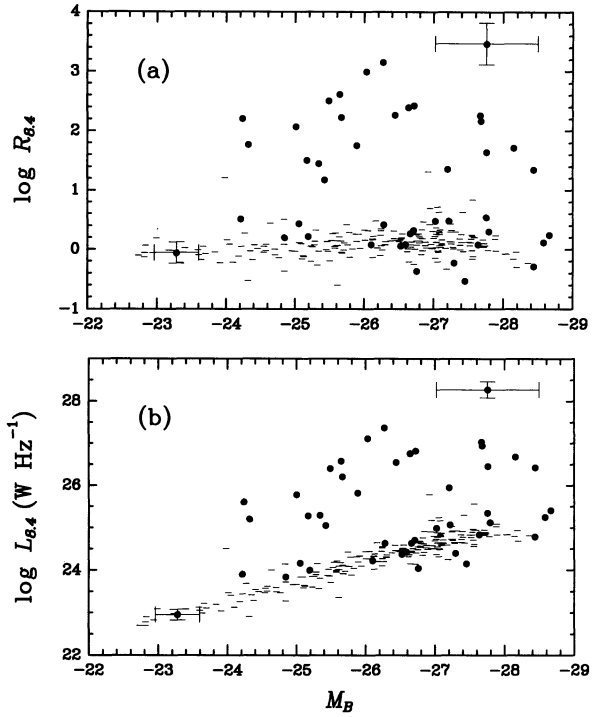

FIG. 4.—The distribution of (*a*) log $R_{8.4}$ and (*b*) log $L_{8.4}$ against M_B. Filled circles represent detections, and horizontal lines are upper limits. Error bars ($\pm 1\,\sigma$), calculated as described in § 2.3, are shown for representative points.

The data are then partitioned into two sections, and the scatter is calculated separately for each section. If the data are intrinsically clumped in two groups, the partition which corresponds to the division between these groups results in a small scatter within each section, relative to the dispersion of the entire data set. Therefore, the maximum, over all possible partitions, of the ratio of total scatter to the sum of the scatter in each of the two sections is a measure of the clumping of the data. This ratio is subsequently maximized over all rotations of the line to obtain

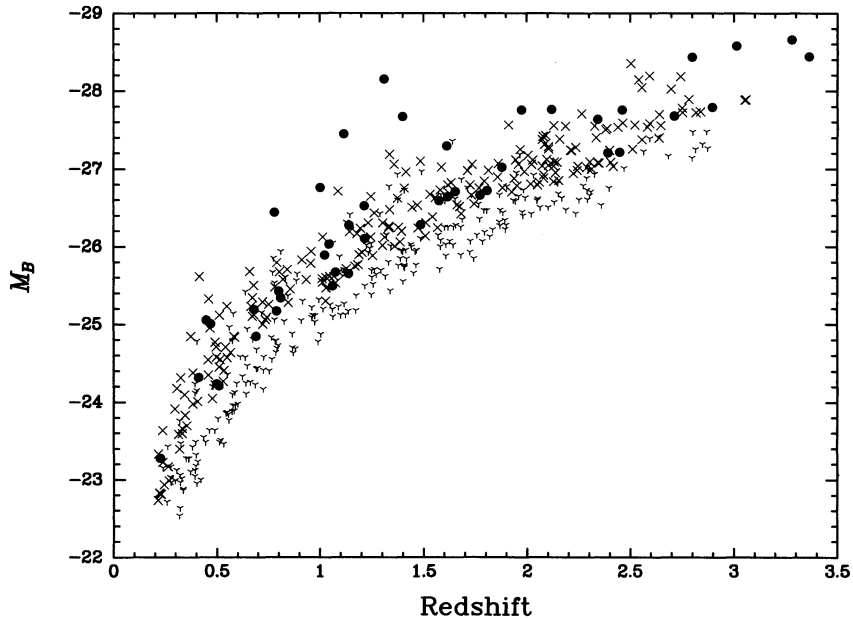

FIG. 3.—Distributions of M_B against redshift for the LBQS radio detections (*filled circles*) and upper limits (*crosses*). Y-shaped symbols represent LBQS quasars without radio observations, only $\frac{1}{3}$ of which are plotted for clarity.

the Lee statistic. Monte Carlo simulations based on an assumed unimodal comparison distribution are used to calibrate the statistic and evaluate the significance of the result. An analysis of three comparison distributions appropriate for the LBQS data is presented in Appendix A.

Stocke et al. (1992) applied the Lee statistic to the distributions of radio luminosity and log R at 5 GHz (log L_5 and log R_5, respectively), derived from Paper I, MPM, and PG, the major radio surveys of optically selected quasars available at the time. All of these samples have log L_5 and log R_5 distributions which were shown to be different from a single Gaussian function (incorporating upper limits) at or above the 98% confidence level, from which Stocke et al. (1992) concluded that the log R_5 and log L_5 distributions are bimodal. Della Ceca et al. (1994) applied the same test as Stocke et al. (1992) to a sample of 406 X-ray–selected quasars with radio data and found evidence for a bimodal distribution of the radio to optical luminosity ratios. The log $R_{8.4}$ distribution of the current, enlarged, LBQS radio sample is also incompatible with a Gaussian distribution (point iii. in Appendix A) at a 99.8% confidence level. The confidence level of the result remains at or above 99% when either the mean or standard deviation are changed by a few tenths.

The results from the Gaussian comparison functions alone do not unequivocably demonstrate that the data have a bimodal distribution. The observed data would have to be inconsistent with all reasonable unimodal distributions to reach such a conclusion. Since testing all potential models is impractical, some of the most stringent tests were performed, using distributions which closely approximate the data, except that the models are unimodal. This has the effect of isolating the feature of interest, the hypothesized gap in the log $R_{8.4}$ distribution, and reducing the influence of differences between the model and the data unrelated to testing for a local minimum. The observed log $R_{8.4}$ data differ from one such model (point ii. in Appendix A) at only a 39% confidence level. Therefore, given the size of the current data set, a Gaussian model is ruled out, but it is not possible to use the Lee statistic to discriminate between a bimodal distribution and a unimodal distribution with an extended tail.

Regardless of whether the log $R_{8.4}$ distribution is truly bimodal, in common with previous work, the high log $R_{8.4}$ tail of the distribution is classified as "radio-loud." A dividing value of log $R_{8.4} = 1$ was chosen to coincide with the apparent gap and for consistency with other studies. PG and Padovani (1993) used the same dividing value, Stocke et al. (1992) adopted log $R_{8.4} = 1.2$, and La Franca et al. (1994) employed a radio to optical spectral index definition equivalent to a division at log $R_{8.4} = 0.86$, assuming an 8.4 GHz to 5 GHz spectral index of -0.5. A corresponding division between loud and quiet in terms of radio luminosity was chosen to be log $L_{8.4} = 25$, close to the radio luminosity of an object with log $R_{8.4} = 1$ and the median absolute magnitude of the sample. The two definitions of radio-loud are not equivalent, especially at low and high optical luminosities. The observed sample has no radio-loud quasars, by either definition, at low optical luminosities, and the only differences in classification of detections occur for $M_B < -27.2$: 0105−2649, 0302−0019, 1235+0857, 1443+0141, 2231−0015 have log $L_{8.4} > 25$ but log $R_{8.4} < 1$.

3.2.2. *Distribution of Radio Luminosity as a Function of M_B*

The radio-loud (log $L_{8.4} > 25$) quasars are distributed relatively uniformly in M_B and log $L_{8.4}$ for $M_B < -24$ (Fig. 4). A BHK correlation test, a Kendall's τ test modified to incorporate upper limits (Isobe, Feigelson, & Nelson 1986), of detections and upper limits with log $L_{8.4} > 25$ showed no significant correlation between M_B and log $L_{8.4}$, consistent with the results of MPM and Stocke et al. (1992).

MPM found evidence that the fraction of quasars with high radio luminosity increases with increasing optical luminosity, a result which is strengthened by combining the MPM sample with data from the first LBQS radio observations (Paper I). A similar result at a 99.6% confidence level is obtained if the test criteria from Paper I, which divided quasars in the redshift range $1 < z < 2.5$ into two absolute magnitude groups separated at $M_B = -27.5$, are applied to the enlarged LBQS sample alone.

Padovani (1993) found that the optical luminosity functions (OLFs) for the full PG sample and the radio-loud (log $R_{8.4} > 1$) subsample have similar cosmological evolutions and a similar shape for bright absolute magnitudes, within the uncertainties of the data. At fainter absolute magnitudes the radio-loud OLF is flatter, resulting in a lower radio-loud fraction. The change in slope occurs at $M_B \approx -24$ for $z = 0$ and at higher optical luminosities with increasing redshift. Analogous results were obtained by Della Ceca et al. (1994) for the X-ray luminosity function (XLF) of X-ray–selected quasars: the radio-loud and radio-quiet XLFs have experienced similar luminosity evolution, and the radio-loud fraction decreases at low X-ray luminosities. The pure luminosity evolution and the local OLFs determined by Padovani (1993) were used to calculate expected radio-loud fractions in the LBQS. The results for high-redshift quasars are ambiguous, since the evolution is undetermined for $z > 2.2$, the redshift cutoff of the PG sample. Two extremes of high-redshift evolution were considered: no evolution for $z > 2.2$; and the same function used for lower redshifts. The predicted radio-loud fractions were not markedly different for these two choices, and both reproduced the overall trend in the data of higher radio-loud fraction at brighter absolute magnitudes. However, the total number of radio-loud quasars predicted is 2.5 times the number observed, and even after normalizing the model to match the observed total, the predicted radio-loud fraction as a function of absolute magnitude does not fit the data well. A χ^2 test for a series of absolute magnitude bins gives a 95% probability that the data and model are incompatible. A somewhat better fit (89%) is obtained by considering only LBQS quasars with $z < 2.2$, but the same qualitative differences between model and data remain.

La Franca et al. (1994) combined several published optically selected quasar samples with radio data and observations of their own for a study of the radio-loud (log $R_{8.4} > 0.86$) fraction. One of the products of this analysis is a series of expected radio-loud fractions in redshift and absolute magnitude bins (their Table 5) based on derived radio-loud and total optical luminosity functions. The model radio-loud fractions increase with brighter absolute magnitudes in each of the redshift ranges. The full LBQS radio sample was found to be inconsistent at the 97% confidence level with these predictions, based on a χ^2 goodness-of-fit test, with some of the bins combined to obtain an expected number of radio-loud (log $R_{8.4} > 0.86$) objects greater than two in each bin. The model predicts a substantially higher radio-loud fraction than is observed for the LBQS ($\approx$25% compared to $\approx$10%) in the redshift range $0 < z < 1$, which is dominated by PG quasars in the La Franca et al. (1994) sample. If low redshifts are not considered, the LBQS data are more compatible (inconsistent at the 87% confidence level) with the expected fractions for $1 < z < 3$.

The fractions of detections with log $L_{8.4} > 25$ and log $R_{8.4} > 1$ are 27/256 (11%) and 22/256 (9%), respectively, for the LBQS sample. A χ^2 test for goodness of fit was used to determine whether the average radio-loud fraction for the sample is consistent with the radio-loud fractions in eight absolute magnitude bins chosen to each contain 32 quasars. The null hypothesis that the fraction of detections with log $L_{8.4} > 25$ is independent of absolute magnitude can be rejected at the 99.6% confidence level. A similar test using the log $R_{8.4} > 1$ definition of radio-loud gives rejection of the null hypothesis at an 88% confidence level. The only differences in the log $L_{8.4}$ and log $R_{8.4}$ distributions occur in the two brightest absolute magnitude bins, which contain a total of five more detections with log $L_{8.4} > 25$ than with log $R_{8.4} > 1$.

A graphical representation of the behavior of the radio-loud fraction as a function of M_B, shown in Figure 5, was constructed by calculating the radio-loud fraction of objects within a 1 mag range centered on the M_B value of each quasar in the sample, essentially a boxcar smoothing of the data. The error bars (± 1 σ) shown at selected values of M_B are the standard deviations of a fraction calculated from a binomial random variable: $\sigma = [f(1-f)/N]^{1/2}$, where f is the radio-loud fraction in a 1.0 mag bin centered on M_B containing N points. The salient features of the functions, namely a value of zero at faint magnitudes, rising to $\sim$15% around $M_B = -25.5$, reaching a minimum for $M_B \sim -27$, climbing to the highest values at the brightest absolute magnitudes, and differences between the log $R_{8.4} > 1$ and log $L_{8.4} > 25$ fractions at bright absolute magnitudes, are present for smoothing scales ranging from 0.5 to 2.0 mag.

The sharp rise in smoothed radio-loud fraction (log $L_{8.4} > 25$) at bright absolute magnitudes and the differences in the χ^2 goodness-of-fit results between log $L_{8.4} > 25$ and log $R_{8.4} > 1$ are suggestive of a greater proportion of luminous radio emitters among optically luminous quasars. The most optically luminous absolute magnitude bin contains 10/32 (31%) detections with log $L_{8.4} > 25$. Given the average radio-loud fraction for the whole sample of 27/256 (11%), the binomial probability of obtaining at least this many radio-loud quasars in one bin is 0.0012. Since no a priori decision was made to test a particular bin, the probability was multiplied by the number of bins (8), for a final confidence level of 99.0%. The fraction of detections with log $R_{8.4} > 1$ in the most optically luminous bin is not significantly different from the average, despite the fact that the smoothed fraction attains its highest value at bright absolute magnitudes.

The relatively high fraction of LBQS quasars with log $L_{8.4} > 25$ at bright absolute magnitudes may be the result of a positive correlation between radio and optical luminosity among the radio-quiet population, as was found in the PG by Stocke et al. (1992). In this scenario, since the radio-loud quasars appear to have no such correlation, the two populations merge at high optical luminosity, resulting in an enhancement in the fraction of quasars with radio luminosity above the "radio-loud" threshold. Stocke et al. (1992) suggested that the radio-quiet correlation could arise if a large portion of the radio emission in these quasars comes from the kinetic energy of outflowing material, such as broad absorption line clouds, driven by optical/UV radiation pressure. There is indirect evidence that the above explanation holds in the LBQS, in that the fraction of radio detections among the radio-quiet quasars remains roughly constant at 5%–10% over the full range of absolute magnitude. If there were no correlation or a negative correlation between the luminosities among the radio-quiet objects, the fraction of detections would decline at higher redshifts (brighter M_B), since the radio luminosity of the 3 σ detection limit increases with z (Fig. 4*b*).

3.2.3. *Evidence for a Change in the Quasar Population at Faint Optical Luminosities*

Peacock et al. (1986) presented evidence for an abrupt change in the radio properties of the quasar population at an

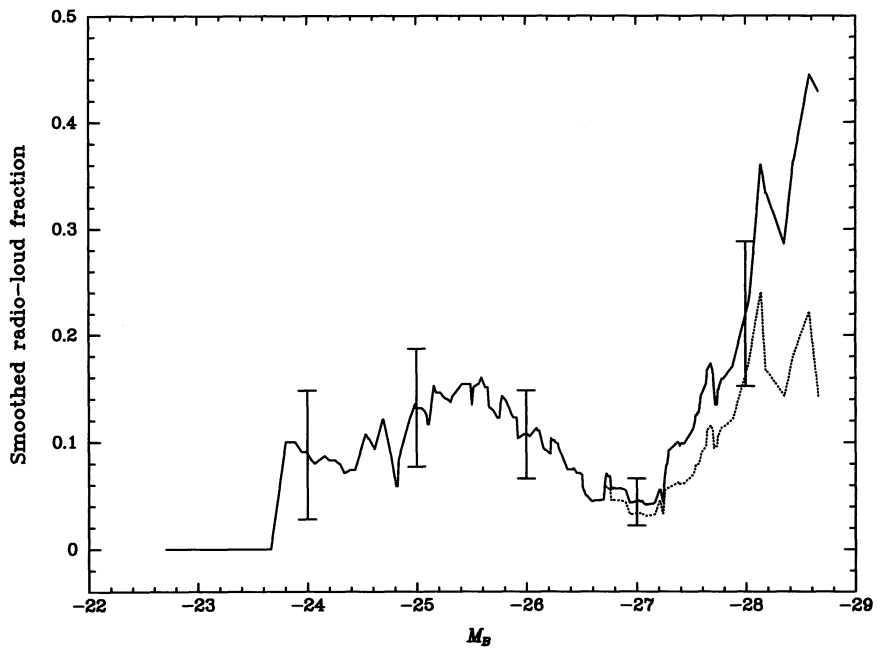

FIG. 5.—Smoothed radio-loud fraction as a function of M_B for a smoothing scale of 1.0 mag. The solid line is the fraction of detections with log $L_{8.4} > 25$, and the dotted line represents the fraction with log $R_{8.4} > 1$. Error bars (± 1 σ), calculated as described in § 3.2.2, are shown at selected absolute magnitudes.

absolute magnitude $M_B \sim -24$, based on the PG survey and a radio-selected sample from the Parkes catalog. In particular, they found a dramatic reduction in the fraction of quasars that were radio-loud at magnitudes $M_B > -24$. None of the PG quasars with $M_B > -24$ is radio-loud ($\log L_{8.4} > 25$), compared to a radio-loud fraction of 24/69 (35%) for the remainder of the survey, a change significant at more than the 99.99% confidence level. This change with absolute magnitude is clearly seen in the luminosity function of the radio-loud PG quasars (Padovani 1993). Although Della Ceca et al. (1994) find some radio-loud quasars with $M_B > -24$ in an X-ray–selected sample, the fraction (3%) is significantly less than for brighter absolute magnitudes (30%) at greater than 99.99% confidence level. Inspection of Figure 4 suggests that the radio properties of the LBQS quasars concur with these results.

The change in the radio distribution for quasars fainter than $M_B = -24$ could be an evolutionary effect. All of the low-luminosity ($M_B \geq -24$) quasars in the LBQS are in the redshift range $0.2 < z < 0.41$ (Table 3). For comparison, the radio-loud fraction is close to 10% for the higher luminosity quasars with $z < 0.5$, although most of these have $z > 0.41$. This suggests that the change in the radio distribution is likely to be caused by differences in M_B rather than z, but the confidence level of the result is only 90% due to the small number of objects involved. The PG sample also has limited overlap in redshift between the bright and faint quasars (Table 3). However, the bright PG quasars provide a closer redshift match for the LBQS quasars fainter than $M_B = -24$. The radio-loud fraction among the optically bright ($M_B < -24$) PG quasars in the range $0.2 < z < 0.41$ is 9/21 (43%), different from the optically faint LBQS sample at greater than 99% confidence level.

Statistical tests comparing the absence of radio-loud quasars at faint absolute magnitudes to the radio-loud fractions of brighter quasars have low confidence levels (91% for $\log L_{8.4} > 25$; 86% for $\log R_{8.4} > 1$). The relatively weak results are due to the small number (20) of LBQS quasars fainter than $M_B = -24$, combined with the low predicted occurrence of radio-loud quasars ($\sim 10\%$), determined from the brighter quasars. However, the VLA observations provide information on the incidence of quasars with radio luminosities considerably fainter than the canonical $\log L_{8.4} = 25$ limit. A significant number of detections for objects with luminosities as faint as $\log L_{8.4} = 23.8$ occur for $M_B < -24$. Upper limits to the radio luminosity are also present above $\log L_{8.4} = 23.8$, but the number of detections places a firm lower limit to the fraction of quasars with radio luminosities exceeding $\log L_{8.4} = 23.8$. At absolute magnitudes brighter than $M_B = -24$, 43/236 (18%) quasars are detected with $\log L_{8.4} > 23.8$. There are 20 quasars with $M_B \geq -24$, with no detections at $\log L_{8.4} > 23.8$ and only one upper limit exceeding this luminosity (1138+0204). Based on the expected fraction of 0.18 from the bright sample for the admittedly a posteriori radio luminosity division $\log L_{8.4} = 23.8$, the binomial probability of observing one or fewer quasars more luminous than $\log L_{8.4} = 23.8$ (assuming the upper limit is detected at $\log L_{8.4} > 23.8$) is 0.098, and (assuming the object with the upper limit is not detected at $\log L_{8.4} > 23.8$) of zero quasars is 0.018.

If more sensitive observations confirm that 1138+0204 has a radio luminosity $\log L_{8.4} < 23.8$, the LBQS sample will provide further evidence of the discontinuity in the radio properties of quasars at $M_B \sim -24$ reported by Peacock et al. (1986).

A potential selection effect may be influencing the observed fraction of radio-loud quasars at faint optical luminosities. The M_B values used in the LBQS analysis include contributions from both quasar and host galaxy. Magnitudes of the quasar alone could be fainter by up to 0.75 mag (factor of 2), since the LBQS selected quasars at least as bright as their host galaxies. Shifts to fainter magnitudes for individual quasars will tend to be greater for fainter M_B, since the relative contribution of the host galaxy will be larger. If, as in the hypothesis of Peacock et al. (1986), the radio-loud quasars lie in elliptical galaxies, which may be intrinsically brighter than the spiral galaxies which host the radio-quiet quasars, then the luminosities of the radio-loud quasars may shift farther to the left in Figure 4 than the radio-quiet quasars. Conceivably, one or more of the three quasars with radio luminosities $\log L_{8.4} > 23.8$ and absolute magnitudes $-24.75 < M_B < -24.0$ could reside in a high-luminosity elliptical galaxy, in which case the nuclear luminosity of the quasar may be fainter than $M_B = -24$.

Peacock et al. (1986) ascribed the origin of the apparent change in the radio-loud fraction at $M_B = -24$ to a systematic difference in the classification of active galactic nuclei, coupled with the existence of two distinct classes of object: radio-quiet quasars which exist primarily in spiral galaxies and radio-loud quasars which reside primarily in elliptical galaxies. In the analysis of quasars taken from radio surveys, they hypothesized that radio-loud quasars with faint optical luminosities are classified as radio galaxies, resulting in a deficiency of optically faint quasars where the elliptical galaxy host appears sufficiently prominent.

This explanation cannot be tested quantitatively with the PG quasars, as the effects of host galaxy type and magnitude on quasar selection probability are not accurately known for this survey. The significance of this selection effect for the identification of quasars in the LBQS was investigated in detail (see Appendix B), an analysis made possible by the survey's broad, well-defined, and consistently applied selection criteria, and the ability to accurately simulate the appearance of a test spectrum on the objective-prism plates. The simulations show that very few quasars residing in elliptical hosts would be missed by the

TABLE 3

RADIO-LOUD FRACTION ($\log L_{8.4} > 25$) AS A FUNCTION OF z AND M_B

Survey	M_B Range	$z < 0.2$	$0.2 < z < 0.41$	$0.41 < z < 0.5$	$0.5 < z < 1.0$	$z > 1.0$
LBQS.....	$M_B > -24$	...	0/20	...	...	...
	$M_B < -24$	...	0/5	2/13 (15%)	5/41 (12%)	20/177 (11%)
PG	$M_B > -24$	0/45[a]	...	...	...	...
	$M_B < -24$	1/17 (6%)	9/21 (43%)	3/5 (60%)	5/7 (71%)	6/19 (32%)[b]

[a] 0/24 for $M_B < -22.7$, the faint absolute magnitude limit of the LBQS.
[b] 1/9 (11%) for $M_B > -28.7$, the bright absolute magnitude limit of the LBQS.

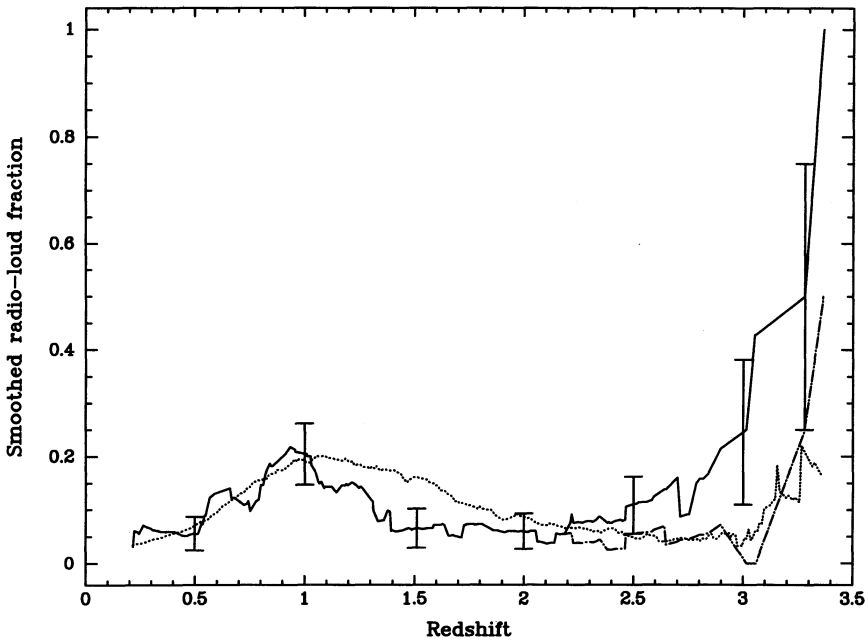

FIG. 6.—Smoothed radio-loud fraction as a function of redshift with a smoothing scale of $\Delta z = 0.5$. The observed fraction of detections with $\log L_{8.4} > 25$, with $\log R_{8.4} > 1$, and predicted by the model derived from the radio luminosity functions of Dunlop & Peacock (1990) are indicated by the solid, dashed, and dotted lines, respectively. Error bars ($\pm 1\ \sigma$), calculated as described in § 3.2.2., are shown at selected redshifts.

LBQS selection algorithms. The revised significance calculation, taking into account the results of the simulation, ascribes a significance of 0.030 (cf. 0.018 above) to observing 0 radio-loud quasars among the 20 $M_B \geq -24$ objects. The simulations are based on a series of conservative (worst case) assumptions, and the results suggest that the hypothesis advanced by Peacock et al. (1986) to explain their own result does not provide a tenable explanation for the lack of optically faint, radio-loud quasars in the LBQS sample.

3.3. *The Evolution of Radio and Optical Luminosity*

The smoothed radio-loud fraction as a function of redshift (Fig. 6) was calculated using the method described in § 3.2.2. for a redshift interval of 0.5. The upturn in radio-loud ($\log L_{8.4} > 25$) fraction for the observed data at high-z and the apparent peak at $z \approx 1$ are present for larger smoothing scales, although the peak becomes broader and less prominent and is hardly visible for a redshift interval of 1.5. The increased fraction of detections with $\log R_{8.4} > 1$ is barely present with larger smoothing intervals. A χ^2 test found that the LBQS sample, divided into eight redshift bins with 32 quasars in each, is inconsistent with an unevolving radio-loud fraction at the 97.2% ($\log L_{8.4} > 25$) and 94% ($\log R_{8.4} > 1$) confidence levels. The only substantial departures from the average radio-loud fractions are overabundances of radio-loud objects in a bin consisting of the redshift interval $0.75 < z < 1.12$ and, for $\log L_{8.4} > 25$ only, the highest redshift bin, $2.41 < z < 3.36$, consistent with the redshifts at which the smoothed fraction is enhanced. A model based on Padovani's (1993) optical luminosity functions (see § 3.2.2.) predicts that the radio-loud ($\log R_{8.4} > 1$) fraction rises slowly with increasing redshift, which, except for the peak around $z = 1$, is consistent with the observed data.

Many of the quasars in the two redshift ranges with increased radio-loud fraction have absolute magnitudes corresponding to the maxima in the radio-loud fraction as a function of M_B (Fig. 5), resulting in an ambiguity as to whether observed changes in radio-loud fraction are primarily evolutionary effects or a function of absolute magnitude. La Franca et al. (1994) found that the radio-loud fraction decreases with redshift for constant M_B (their Table 5). The MPM sample is well suited to resolve the ambiguity in the cause of the elevated radio-loud fraction at $z \approx 3$ and at $z \approx 1$, since that sample is confined to a redshift range ($1.8 < z < 2.5$) between the redshifts of these peaks and has an absolute magnitude coverage ($-28.4 < M_B < -25.0$) which includes the absolute magnitudes of the peaks. Absolute magnitudes for the MPM quasars were calculated in the same manner as for the LBQS, after apparent B magnitudes were derived from m_{1475} as described in La Franca et al. (1994). The smoothed radio-loud fraction for the MPM data, calculated with a 1.0 magnitude smoothing range, is flat within the error bars from $M_B = -25$ to -27, at which point the fraction rises steeply, consistent with the rise at bright absolute magnitudes in the LBQS sample. Lack of a local maximum at $M_B \approx -25.5$ suggests that the peak observed at these absolute magnitudes in the LBQS is caused by an increase in radio-loud fraction for $z \approx 1$. In summary, the causal variable for the upturn in radio-loud fraction appears to be absolute magnitude at $z \approx 3$ and redshift at $z \approx 1$, although the current LBQS radio subsample is insufficient to resolve this issue conclusively.

An independent estimate of the evolution of the radio-loud fraction was obtained from the 2.7 GHz luminosity function models of Dunlop & Peacock (1990). The expected radio-loud fraction in any redshift interval, $z_1 < z < z_2$, is proportional to the double integral of the radio luminosity function (RLF) over (z_1, z_2) and the luminosity range $\log L_{8.4} > 25$ divided by the number of optically selected quasars in this redshift range. The lower luminosity limit is equivalent to a 2.7 GHz luminosity of $10^{24.15}$ W Hz^{-1} sr^{-1}, assuming a spectral index of -0.5 and a factor of 4π to convert to the luminosity units used in Dunlop & Peacock (1990). LBQS quasars in the apparent magnitude

range of the radio subsample, $16.0 < B < 18.5$ (Fig. 1), were used for the count of optically selected quasars. The same apparent magnitude criteria were incorporated into the RLF by multiplying the integral by the fraction of radio-selected quasars having apparent magnitudes in the above range and redshifts in (z_1, z_2), determined from the more than 1100 radio-selected quasars with redshifts and apparent V magnitudes listed in the latest version of the Hewitt & Burbidge Catalog (1993). $B-V$ colors from Cristiani & Vio (1990) were used for the cataloged quasars without measured colors, as the LBQS composite spectrum does not extend sufficiently to the red to calculate $B-V$ colors. Model radio-loud fractions were normalized by requiring that the calculated fraction for the redshift range of the LBQS radio sample equal the observed average fraction.

Radio-loud fractions were calculated from the flat-spectrum MEAN-z model RLF1 of Dunlop & Peacock (1990) for the redshift intervals resulting from the division of the LBQS radio sample into eight redshift bins of 32 quasars each. Although a χ^2 test indicates that the model is inconsistent with the observed data for the eight bins at the 99.7% confidence level, the predicted numbers of radio-loud ($\log L_{8.4} > 25$) quasars are close to the observed values in all but the highest redshift bin ($2.41 < z < 3.36$), in which 1.6 are predicted, compared to seven observed. The discrepancy in the high-redshift range is responsible for the high confidence level from the χ^2 test; if only the first seven bins are used, the model is not rejected by the test. The model rather closely reproduces the local maximum at $z \approx 1$ seen, along with the discrepancy at high redshift, in the smoothed radio-loud fraction (dotted line in Fig. 6), calculated for the model in an analogous manner to that employed for the observed data.

The divergence of the model and data for $z > 2.5$ can be understood if optical luminosity is the causal variable for the enhanced radio-loud fraction at bright absolute magnitudes. In this case the increase in the fraction at high redshift results from the preponderance of optically luminous objects among the high-redshift quasars in the radio sample. Otherwise, the discrepancy between model and data is unexplained. The slight upturn in model smoothed fraction for $z > 3$ may arise from the change in the evolution of the luminosity function of optically selected quasars for $z \gtrsim 3$: Hewett, Foltz, & Chafee (1993) found that the few LBQS quasars with $z > 3$ are consistent with a constant space density at these redshifts, and Warren et al. (1994) concluded that the space density declines for $z > 3.3$. Sharp variations in the smoothed fraction at these redshifts result from small number statistics in the apparent magnitude correction factor to the RLF and in the number of LBQS quasars in the smoothing interval.

Radio luminosity and $\log R_{8.4}$ are plotted against redshift and lookback time in Figure 7. The radio-loud LBQS detections and upper limits show no significant correlation between redshift and $\log L_{8.4}$ or $\log R_{8.4}$. The LBQS was supplemented at high redshift with data from McMahon, Irwin, & Hazard (1992) and Schneider et al. (1992), also shown in Figure 7. McMahon et al. (1992) used the VLA to observe 29 optically selected quasars with $3.5 < z < 4.7$ and $M_B < -26$, detecting four of these quasars at 5 GHz. Individual redshifts and magnitudes were not published. Any biases in the sample selection are unknown. The four detections, which have $z < 4.25$, are indicated by lines of constant 8.4 GHz luminosity and $\log R_{8.4}$ in Figure 7. The published R values for the detections, defined as the ratio of 5 GHz to V-band flux, were converted to $R_{8.4}$ assuming an optical spectral index of 0.0 and a radio spectral index of -0.5. The dotted line in each panel shows the 8.4 GHz luminosity and $\log R_{8.4}$ values corresponding to the 3 σ upper limit of 0.5 mJy in McMahon et al. (1992) as a function of redshift. Schneider et al. (1992) state that their sample of 22 optically selected quasars in the absolute magnitude range $-27.3 < M_B < -24.9$ drawn from the literature is incomplete, but they believe that the radio properties are unbiased. They detected only one object at 5 GHz at a 5 σ limit of $\approx$0.21 mJy. The detection and the individual upper limits, converted to 8.4 GHz, are represented in Figure 7 by an asterisk and crosses, respectively.

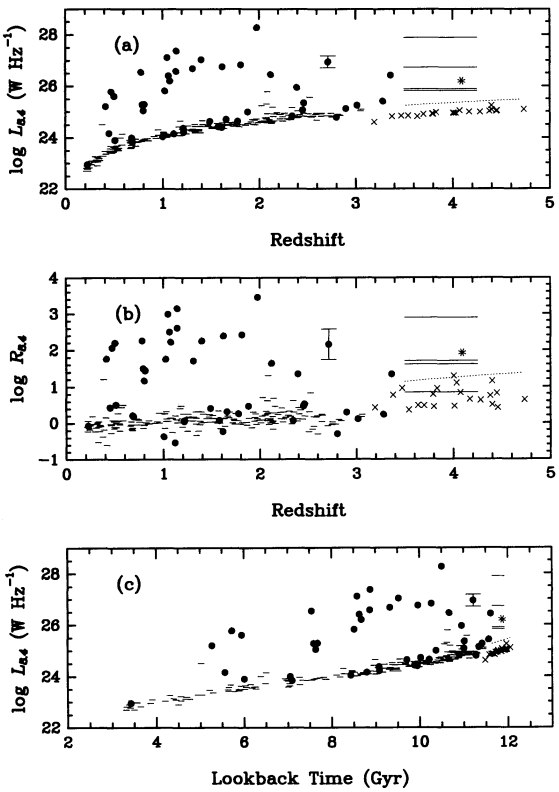

FIG. 7.—The distribution of (*a*) $\log L_{8.4}$ and (*b*) $\log R_{8.4}$ against redshift, and (*c*) $\log L_{8.4}$ against look-back time. Filled circles and short dashes represent LBQS detections and upper limits, respectively. The asterisk is the Schneider et al. (1992) high-redshift detection, and their 5 σ upper limits are shown as crosses. The solid lines indicate the redshift range and the radio luminosity or $\log R_{8.4}$ value for the four detections in McMahon et al. (1992). The nondetections in McMahon et al. (1992) are displayed collectively by the dotted line as a range of upper limits in $\log L_{8.4}$ or $\log R_{8.4}$. Error bars ($\pm 1\ \sigma$) for $\log L_{8.4}$ and $\log R_{8.4}$, calculated as described in § 2.3., are shown for a representative high-redshift point in each panel. Low-redshift error bars are of order the size of the filled circles.

The radio-loud ($\log L_{8.4} > 25$) fraction in the combined McMahon et al. (1992) and Schneider et al. (1992) data sets is 5/51 (10%), consistent with the LBQS radio-loud fraction in the redshift range $1.5 < z < 2.5$. The absolute magnitude range of these lower redshift LBQS quasars (see Fig. 3) is similar to that of the Schneider et al. (1992) data, and there is overlap with the McMahon et al. (1992) objects, although some of the quasars in the latter sample may have substantially higher optical luminosities. The simplest interpretation of all of the observations is that the radio-loud fraction of quasars with $M_B \gtrsim -28$ is 5%–10% from $z \approx 1.5$ to redshifts close to 5. A

direct test of this interpretation would require a larger sample of quasars with $z > 2.5$ and $M_B > -28$.

4. SUMMARY

The evolution of radio luminosity with cosmic epoch and its relationship with optical luminosity for optically selected quasars has been investigated, with the following principal results.

i. There is a significant deficit of optically faint ($M_B \geq -24$) quasars with radio luminosities detectable at the flux limits of the LBQS VLA study. This effect appears to be the result of a real physical change in the quasar population, since it cannot be accounted for by an LBQS selection bias against quasars which have large radio luminosities and small optical luminosities. The deficit of optically faint, radio-loud quasars does not appear to be an evolutionary effect, since the change is present among quasars of similar redshifts.

ii. The radio-loud fraction (log $L_{8.4} > 25$) of LBQS quasars is approximately 10%, independent of absolute blue magnitude, in the range $-27.5 \lesssim M_B \lesssim -24$, and rises sharply for brighter absolute magnitudes. An observed increase in the fraction around $M_B \approx -25.5$ is more likely a manifestation of an enhanced radio-loud fraction at $z \approx 1$. No significant correlation between M_B and log $L_{8.4}$ is present among the radio-loud quasars.

iii. The radio-loud fraction exhibits a peak around $z \approx 1$, is constant at $\approx 10\%$ until $z \approx 2.5$, and then increases substantially to $z = 3.4$, the highest redshift in the LBQS. A model based on radio luminosity functions produces a good match to the data for $z \lesssim 2.5$ but predicts too low a fraction at higher redshifts. The radio-loud fraction at $z > 3.5$, based on data from the literature, is $\approx 10\%$, similar to that in the range $1.5 \lesssim z \lesssim 2.5$. There is evidence that the enhanced observed radio-loud fraction at $z \approx 3$ may be a result of increased radio-loud fraction at bright absolute magnitudes (see point ii. above), which would explain the discrepancy between the data and the model and indicate that the radio-loud fraction is roughly constant from $z \approx 1.5$ to redshifts approaching 5. No significant correlation between z and log $L_{8.4}$ is present among the radio-loud quasars.

iv. The log $R_{8.4}$ distribution may be bimodal. A Gaussian model is clearly not consistent with the observed data, but the sample size is insufficient to determine the applicability of other classes of unimodal distributions.

v. PG quasars have substantially higher radio-loud fraction than the LBQS for M_B brighter than -24 over the redshift range in common to the two samples. A similar discrepancy exists between the PG and other samples, which has led to the conclusion that the radio-loud fraction decreases for $z > 1$, compared to lower redshifts (e.g., Paper I; La Franca et al. 1994). La Franca et al. (1994) note that their combined sample is consistent with no evolution in the radio-loud fraction among $z > 1$ quasars if the PG is excluded. The expanded LBQS sample contains a large number of quasars with $z < 1$, and the strong evolution between low and high redshifts indicated by the PG is not seen. The reason for the enhanced radio-loud fraction in the PG, relative to other optically selected quasar samples, is unknown.

The authors thank Stephen Warren for calculating the high redshift k-corrections, Karen Visnovsky and Paul Francis for helpful discussions, and Ken Kellerman for a thought-provoking question. Joan Wrobel provided assistance with the reduction of the VLA data. The referee, John Stocke, made insightful and useful comments and suggestions. This work was partially supported by NSF grants AST 90-01181 and AST 93-20715 and NASA grant NGT-51152. This research has made use of the NASA Astrophysics Data System (ADS) and the NASA/IPAC Extragalactic Database (NED), operated by the Jet Propulsion Laboratory, California Institute of Technology, under contract with the National Aeronautics and Space Administration.

APPENDIX A

TESTS FOR A BIMODAL DISTRIBUTION

The effectiveness of the Lee statistic in determining whether a set of observed data has a bimodal distribution depends on the ability of the statistic to distinguish between a unimodal distribution and one with similar overall shape containing a local minimum. The discrimination between unimodal and bimodal in general depends on the distribution of the observed data, the number of points in the sample, and the assumed comparison distribution. For illustration, the Lee statistic was evaluated for 1000 realizations of each of a pair of simple unimodal and bimodal log $R_{8.4}$ distributions having the rough characteristics of and the same number of data points as the LBQS log $R_{8.4}$ sample. Each log $R_{8.4}$ value was paired with an absolute magnitude chosen from a model based on the observed distribution of M_B. Upper limits were treated the same as detections in evaluating the statistic. The set of values of the Lee statistic for the unimodal comparison distribution establishes the significance of the result for each test data set drawn from the bimodal population. The fraction of Lee values in the comparison set less than the value for the test is the confidence level that the test data set is *not* consistent with the comparison distribution. A large number of test data sets establishes a range of confidence levels, useful for evaluating the utility of the statistic in differentiating two populations. Results for three illustrative pairs of distributions are described below and plotted in Figure 8. Each distribution was normalized by requiring that the cumulative probability over all values of log $R_{8.4}$ be unity.

i. The simplest comparison is between a uniform probability distribution over the observed log $R_{8.4}$ range, $-0.6 <$ log $R_{8.4} <$ 3.6 (solid line in Fig. 8*a*), and the same distribution with zero probability in the range of the observed gap, $0.5 <$ log $R_{8.4} < 1.2$ (dotted line in Fig. 8*a*). The chance of finding an object with any other value of log $R_{8.4}$ is zero. The distribution with the gap shows evidence for being bimodal, since 83% of the realizations are different from the unbroken comparison distribution at or above the 95% confidence level.

ii. A hybrid model consisting of a probability function based on the observed log $R_{8.4}$ distribution for log $R_{8.4} < 0.5$, and a constant probability for higher values, is a closer approximation to the observed data and hence a better test of the utility of the Lee

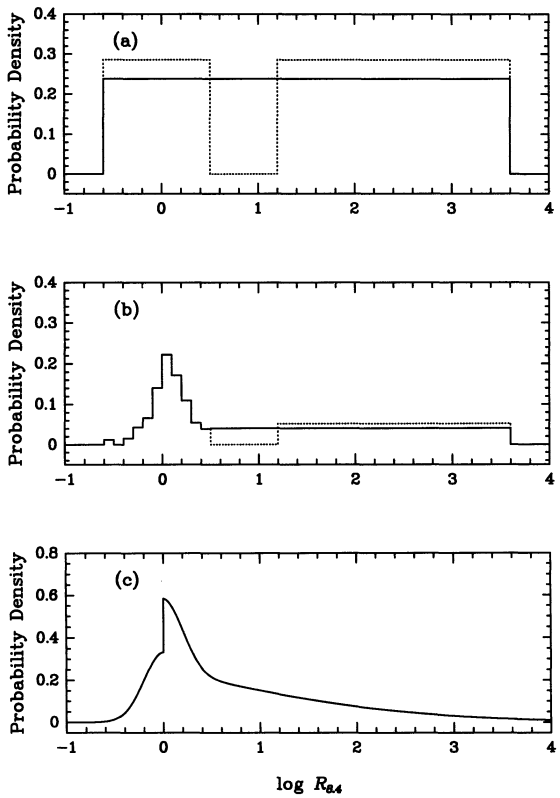

FIG. 8.—Functions employed in tests for a bimodal distribution. Panel (*a*) contains a simple bimodal distribution (*dotted line*) and a uniform comparison distribution (*solid line*). The model in (*b*) is a hybrid of observed LBQS data joined to a uniform probability function with (*dotted line*) and without (*solid line*) a gap between the two distributions. A Gaussian-based model is shown in (*c*).

statistic. The value of the constant probability was chosen to match the observed fraction of objects with $\log R_{8.4} > 0.5$. This model is displayed as the solid line in Figure 8*b*, with the observed data represented by bins of width 0.1 in $\log R_{8.4}$. The dotted line represents the same model, except for a region of zero probability in the range $0.5 < \log R_{8.4} < 1.2$. The statistic is not as successful at distinguishing the hybrid model with and without the gap; only 34% of the test data sets have values of the Lee statistic exceeding the 95% confidence level.

iii. The hybrid model with a gap was also compared to a Gaussian with a mean of -2.2 and standard deviation of 2.3 in $\log R_{8.4}$, selected to match the range of the observed values of $\log R_{8.4}$ and the fraction of quasars in the sample with $\log R_{8.4} > 1$. A detection limit of $\log R_{8.4} = 0 \pm 0.2$ was imposed to correspond to the observed sample. The statistic exceeded the 95% confidence level in 50% of the realizations of the hybrid model. There is a discontinuity in the Gaussian-based model at $\log R_{8.4} = 0$ (Fig. 8*c*) resulting from the imposed detection threshold, which allows upper limits of $\log R_{8.4} > 0$ but excludes detections with $\log R_{8.4} < 0$. The shape of the function near $\log R_{8.4} = 0$ is similar to the probability distribution of the observed data (cf. Fig. 8*b*), although the value of the function is approximately a factor of 2 higher, a result of constraining the Gaussian to accurately reproduce the radio-loud ($\log R_{8.4} > 1$) fraction.

A similar idealized test of a large ensemble of data sets to give the full range of significance levels for each comparison function is not possible with observed $\log R_{8.4}$ data, since the true distribution is unknown, and the number of available empirical "realizations" is limited. However, the basic method of comparing the value of the Lee statistic for an observed sample to a set of values from a comparison distribution to determine a confidence level is unchanged.

The effectiveness of the Lee statistic applied to the LBQS radio sample is limited by the relatively narrow apparent gap in $\log R_{8.4}$ and by the small number of quasars expected to have $\log R_{8.4}$ values in the range of this gap under the null hypothesis of a unimodal distribution. Simulations indicate that the Lee statistic often cannot distinguish between a unimodal $\log R_{8.4}$ distribution similar to that observed (ii. above) and one with a local minimum.

APPENDIX B

HOST GALAXY SELECTION EFFECTS

Selection of LBQS candidates with redshift less than about 2 depends primarily on the color of the object as derived from its objective-prism spectrum. Since elliptical galaxies are redder than quasars, if an elliptical host galaxy were sufficiently luminous the quasar plus elliptical objective-prism spectrum could be reddened enough that it would fail the color-selection criterion.

Simulated spectra consisting of weighted sums of quasar and elliptical galaxy template spectra were constructed to examine the sensitivity of the LBQS selection criteria to a population of relatively optically faint quasars within giant elliptical host galaxies. The host galaxy template chosen for the simulations is the reddest elliptical (NGC 3379; $B-V = 0.95$) in the spectral atlas of Kennicutt (1992). Data from Burstein et al. (1988) were used to extend the spectral coverage into the ultraviolet. Using a red elliptical is conservative, in that rest frame optical colors of quasar host galaxies tend to be bluer than those of normal ellipticals (e.g., Hutchings 1987). The composite quasar spectrum of Francis et al. (1991) was used as the quasar template. Two simulated spectra were created by applying different relative scalings to the quasar and elliptical galaxy templates before co-adding; the quasar had the same absolute B magnitude as the galaxy in one and was 0.25 magnitudes brighter in the other. Only a small percentage of quasars with $M_B < -23$ have host galaxies which are more luminous than the quasar (e.g., Véron-Cetty & Woltjer 1990). The simulation did not include morphological information, because the LBQS selection criteria were applied irrespective of the morphological classification of the image on the direct plates, as long as the quasar flux equalled or exceeded that of the host galaxy.

Each quasar plus elliptical spectrum was redshifted to produce observed-frame spectra for the range $0.0 < z < 0.6$. The redshifted spectra were then transformed to simulate their appearance on a typical objective-prism plate, including the effects of atmospheric extinction, seeing, sensitivity of the IIIaJ emulsion and the nonlinear dispersion of the objective prism. The transformation was derived empirically by matching ~ 100 flux-calibrated spectra of LBQS candidates taken at the Multiple Mirror Telescope to their corresponding spectra on the objective-prism plate. The resulting transformation function produces synthetic objective-prism spectra that are indistinguishable from the actual spectra. Colors of the synthetic spectra were then calculated in exactly the same way as in the generation of the LBQS candidate list (Hewett et al. 1995).

Color tracks of the redshifted synthetic spectra are shown as solid lines in Figure 9, with the upper, redder track corresponding to the case in which the quasar and its host galaxy have equal rest-frame B magnitudes. Redshift is listed along the abscissa, the ordinate is the color estimate derived from objective-prism spectra, with lower numbers indicating bluer colors, and the dashed horizontal line represents the color boundary used to select quasar candidates for spectroscopic follow-up. The region below this line has been explored extensively, whereas few objects above the line have been selected for follow-up spectroscopy on the basis of their color. Quasars above the boundary, such as objects with $z > 2.5$, are identified by the presence of strong emission lines or continuum breaks. The upper color track crosses the selection boundary at $z = 0.24$, implying that the equal-brightness test object would be selected for redshifts $z > 0.24$. A quasar 0.25 magnitudes brighter than the host galaxy (lower track in Fig. 9) would be selected for $z > 0.18$, a redshift range which includes all of the LBQS quasars. Filled circles in Figure 9 represent LBQS quasars selected by color and/or spectral features from the plate used to determine the transformation for the simulated spectra.

The probability of selecting a quasar as a function of the ratio of quasar to host galaxy luminosity was used to estimate the expected fraction of quasars with $M_B \geq -24.0$ having $\log L_{8.4} > 23.8$ in the LBQS. All quasars with $\log L_{8.4} > 23.8$ were assumed to have elliptical host galaxies, with the remainder residing in spirals. The selection probability equals the probability that the

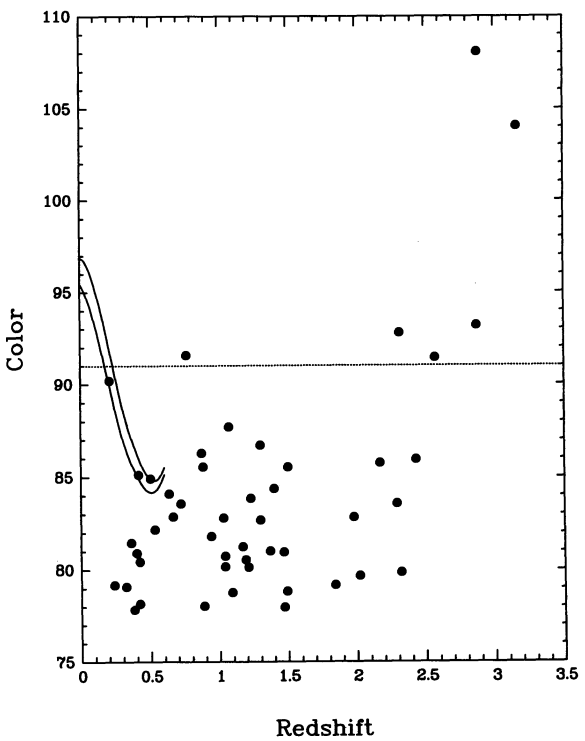

FIG. 9.—Color derived from an objective-prism LBQS plate plotted against redshift. Larger color values represent redder objects. The horizontal line is the LBQS color-selection boundary for this plate. Confirmed quasars and active galactic nuclei are represented by filled circles. The colors of two synthetic quasar plus elliptical spectra as functions of redshift are shown as solid lines crossing the color-selection boundary at $z = 0.18$ and $z = 0.24$.

quasar is brighter than the host galaxy for $z > 0.24$ and at least 0.25 magnitudes brighter for $z < 0.24$. The distribution of quasar to host galaxy optical luminosity ratios was drawn from the literature (Romanishin & Hintzen 1989; Hutchings 1987; Smith et al. 1986; Gehren et al. 1984), subject to the following restrictions: the quasars were radio-selected to avoid a potential optical selection bias against faint quasars in bright host galaxies; the total magnitude of the host galaxy and quasar was fainter than $M_B = -24$; the magnitude of the quasar alone was brighter than an absolute blue magnitude of -22, corresponding to the faintest total M_B in the LBQS radio sample if the quasar and host galaxy contribute equally to the total. The quasar is brighter than its host galaxy in 92% of the cases and is at least 0.25 magnitudes brighter for 77% of the objects.

The likelihood of selecting a quasar with $\log L_{8.4} > 23.8$, $P(\text{select} \mid \text{radio})$, is related by Bayes's theorem to the probability, $P(\text{radio} \mid \text{select})$, that a quasar selected by the survey meets this radio luminosity criterion:

$$P(\text{radio} \mid \text{select}) = \frac{P(\text{select} \mid \text{radio})P(\text{radio})}{P(\text{select} \mid \text{radio})P(\text{radio}) + P(\text{select} \mid \overline{\text{radio}})[1 - P(\text{radio})]}; \quad \text{(B1)}$$

$P(\text{select} \mid \text{radio})$ is 0.92 for quasars with $z > 0.24$ and 0.77 for $z < 0.24$, as determined from the analysis of the LBQS selection criteria. $P(\text{radio})$ is the unconditional probability that a quasar has $\log L_{8.4} > 23.8$, and $P(\text{select} \mid \overline{\text{radio}})$ is the probability of selecting an object with lower radio luminosity, assumed to be unity, a conservative estimate, since a lower probability would raise $P(\text{radio} \mid \text{select})$. The results for $P(\text{radio} \mid \text{select})$ are 0.146 and 0.170 for low and high redshifts, respectively, using $P(\text{radio}) = 43/236(18\%)$, the fraction of $M_B < -24$ detections with $\log L_{8.4} > 23.8$.

Of the 20 quasars in the LBQS radio subsample with $M_B \geq -24$, eight have $z < 0.24$. The expected number of quasars with $\log L_{8.4} > 23.8$ is $8 \times 0.146 + 12 \times 0.170 = 3.21$. The binomial probability of finding 0/20 quasars exceeding this radio luminosity when 3.21 are expected is 0.030, a result insensitive to the exact value of the redshift at which the selection criteria change. For example, if the redshift division had been 0.3, the final probability would change by less than 0.01.

REFERENCES

Aller, M. F., Aller, H. D., & Hughes, P. A. 1992, ApJ, 399, 16
Bennett, C. L., Lawrence, C. R., Burke, B. F., Hewitt, J. N., & Mahoney, J. 1986, ApJS, 61, 1
Burstein, D., Bertola, F., Buson, L. M., Faber, S. M., & Lauer, T. R. 1988, ApJ, 328, 440
Coleman, C. S., & Dopita, M. A. 1992, Proc. Astron. Soc. Australia, 10, 107
Condon, J. J., O'Dell, S. L., Puschell, J. J., & Stein, W. A. 1981, ApJ, 246, 624
Cristiani, S., & Vio, R. 1990, A&A, 227, 385
Della Ceca, R., Zamorani, G., Maccacaro, T., Wolter, A., Griffiths, R., Stocke, J. T., & Setti, G. 1994, ApJ, 430, 533
Dunlop, J. S., & Peacock, J. A. 1990, MNRAS, 247, 19
Dunlop, J. S., Peacock, J. A., Savage, A., Lilly, S. I., Heasley, J. N., & Simon, A. J. B. 1989, MNRAS, 238, 1171
Fitchett, M. 1988, MNRAS, 230, 161
Francis, P. J. 1993, ApJ, 407, 519
Francis, P. J., Hewett, P. C., Foltz, C. B., Chaffee, F. H., Weymann, R. J., & Morris, S. L. 1991, ApJ, 373, 465
Francis, P. J., Hooper, E. J., & Impey, C. D. 1993, AJ, 106, 417
Gehren, T., Fried, J., Wehinger, P. A., & Wyckoff, S. 1984, ApJ, 278, 11
Hawkins, M. R. S. 1986, MNRAS, 219, 417
Hewitt, A., & Burbidge, G. 1993, ApJS, 87, 451
Hewett, P. C., & Foltz, C. B. 1994, PASP, 106, 113
Hewett, P. C., Foltz, C. B., & Chaffee, F. H. 1993, ApJ, 406, 43
———. 1995, AJ, in press
Hook, I. M., McMahon, R. G., Boyle, B. J., & Irwin, M. J. 1994, MNRAS, 268, 305
Hutchings, J. B. 1987, ApJ, 320, 122
Isobe, T., Feigelson, E. D., & Nelson, P. I. 1986, ApJ, 306, 490
Kellermann, K. I., Sramek, R., Schmidt, M., Shaffer, D. B., & Green, R. 1989, AJ, 98, 1195 (PG)
Kennicutt, R. C. 1992, ApJS, 79, 255
Kühr, H., Pauliny-Toth, I. I. K., Witzel, A., & Schmidt, J. 1981a, AJ, 86, 854
Kühr, H., Witzel, A., Pauliny-Toth, I. I. K., & Nauber, U. 1981b, A&AS, 45, 367
La Franca, F., Gregorini, L., Cristiani, S., De Ruiter, H., & Owen, F. 1994, AJ, in press
Lee, K. L. 1979, J. Am. Statistical Assoc., 74, No. 367, 708
Marshall, H. L. 1987, ApJ, 316, 84
McMahon, R. G., Irwin, M. J., & Hazard, C. 1992, in X-Ray, Emission from Active Galactic Nuclei and the Cosmic X-Ray Background, ed. W. Brinkmann & J. Trümper (Garching: Max-Planck-Institut für extraterrestrische Physik), 399
Miller, L., Peacock, J. A., & Mead, A. R. G. 1990, MNRAS, 244, 207 (MPM)
Møller, P., & Warren, S. J. 1991, in The Space Distribution of Quasars, ed. D. Crampton (San Francisco: ASP), 96
Morris, S. L., Weymann, R. J., Anderson, S. F., Hewett, P. C., Foltz, C. B., Chaffee, F. H., Francis, P. J., & MacAlpine, G. M. 1991, AJ, 102, 1627
Orr, M. J. L., & Browne, I. W. A. 1982, MNRAS, 200, 1067
Padovani, P. 1993, MNRAS, 263, 461
Pauliny-Toth, I. I. K., Witzel, A., Preuss, E., Kühr, H., Kellermann, K. I., Fomalont, E. B., & Davis, M. M. 1978, AJ, 83, 451
Peacock, J. A., Miller, L., & Longair, M. S. 1986, MNRAS, 218, 265
Romanishin, W., & Hintzen, P. 1989, ApJ, 341, 41
Sandage, A. 1965, ApJ, 141, 1560
Scheuer, P. A. G., & Readhead, A. C. S. 1979, Nature, 277, 182
Schmidt, M. 1970, ApJ, 162, 371
Schmidt, M., & Green, R. F. 1983, ApJ, 269, 352
Schneider, D. P., van Gorkom, J. H., Schmidt, M., & Gunn, J. E. 1992, AJ, 103, 1451
Smith, E. P., Heckman, T. M., Bothun, G. D., Romanishin, W., & Balick, B. 1986, ApJ, 306, 64
Spinrad, H., Djorgovski, S., Marr, J., & Anguilar, L. 1985, PASP, 97, 932
Sramek, R. A., & Weedman, D. W. 1980, ApJ, 238, 435
Stocke, J. T., Morris, S. L., Weyman, R. J., & Foltz, C. B. 1992, ApJ, 396, 487
Véron-Cetty, M. P., & Woltjer, L. 1990, A&A, 236, 69
Visnovsky, K. L., Impey, C. D., Foltz, C. B., Hewett, P. C., Weymann, R. J., & Morris, S. L. 1992, ApJ, 391, 560 (Paper I)
Wall, J. V., & Peacock, J. A. 1985, MNRAS, 216, 173
Warren, S. J., Hewett, P. C., & Osmer, P. S. 1994, ApJ, 421, 412
Wehrle, A. E., Morabito, D. D., & Preston, R. A. 1984, AJ, 89, 440